PSCAD/EMTDC-BASED MODELING AND ANALYSIS OF A MICROGRID WITH RENEWABLE ENERGY SOURCES

A Thesis

by

ZHENGGUO CHU

Submitted to the Office of Graduate Studies of
Texas A&M University
in partial fulfillment of the requirements for the degree of

MASTER OF SCIENCE

May 2010

Major Subject: Electrical Engineering

PSCAD/EMTDC-BASED MODELING AND ANALYSIS OF A MICROGRID WITH RENEWABLE ENERGY SOURCES

A Thesis

by

ZHENGGUO CHU

Submitted to the Office of Graduate Studies of
Texas A&M University
in partial fulfillment of the requirements for the degree of

MASTER OF SCIENCE

Approved by:

Chair of Committee,	Karen L. Butler-Purry
Committee Members,	Mehrdad Ehsani
	Takis Zourntos
	John Hurtado
Head of Department,	Costas Georghiades

May 2010

Major Subject: Electrical Engineering

ABSTRACT

PSCAD/EMTDC-Based Modeling and Analysis of a Microgrid with Renewable Energy Sources. (May 2010)

Zhengguo Chu, B.E., Tsinghua University

Chair of Advisory Committee: Dr. Karen L. Butler-Purry

Microgrid is a relatively new concept which has gained significant attention recently due to the increasing penetration of distributed energy sources. It brings many benefits to the traditional distribution system. Couples of microgrid testbeds in the forms of either hardware facilities or software simulation systems have been developed to study microgrid issues in many institutes throughout the world.

In the work presented in this thesis, a microgrid system model in PSCAD/EMTDC was developed. The proposed microgrid system includes fundamental power system component models, two renewable energy source models (wind & solar) and one energy storage source model.

Different case studies were conducted. The results from the simulation case studies showed that the proposed microgrid system in PSCAD had satisfactory performance under different scenarios with renewable energy sources. The proposed microgrid system model can be used for further research on microgrid issues.

DEDICATION

To my family and friends,

Thank you for your continued support and love.

ACKNOWLEDGEMENTS

I would like to thank my committee chair, Dr. Karen L. Butler-Purry, for her support and guidance throughout my research work. I have learned many invaluable lessons from her.

I would also like to thank my committee members, Dr. Mehrdad Ehsani, Dr. Takis Zourntos and Dr. John Hurtado, for taking the time and effort to serve on my committee and for their suggestions and feedback for the work of my thesis.

I want to give my gratitude to my colleagues in the Power System Automation Laboratory (PSAL). I have learned much valuable knowledge during my two years in PSAL.

Thanks also go to my friends and classmates and the department faculty and staff for making my time at Texas A&M University a great experience.

Finally, thanks to my parents, my elder sister and brother for their continued encouragement, patience and love.

NOMENCLATURE

AWG	American Wire Gauge
CERTS	The Consortium for Electric Reliability Technology Solutions
DER	Distributed Energy Resource
DG	Distributed Generation
DS	Distributed Storage
EMTDC	Electro-Magnetic Transients in DC Systems
ESS	Energy Storage Source
LL	Line-to-Line
MPPT	Maximum Power Point Tracking
KERI	Korea Electrotechnology Research Institute
PLL	Phase-Lock-Loop
RES	Renewable Energy Source
PSCAD	Power System Computer Aid Design
PV	Photovoltaic
PWM	Pulse-Width Modulation
SLG	Single-Line-to-Ground

TABLE OF CONTENTS

Page

LIST OF FIGURES

Page

Page

Page

LIST OF TABLES

1. INTRODUCTION

1.1. Introduction

A microgrid is a system that has at least one distributed energy resource (DER) and associated loads in it and can form intentional island in electrical distribution system [1]. A microgrid should be able to operate in two different modes: grid-connected mode and islanded mode (also defined as autonomous mode). Microgrids bring many benefits for integrating distributed energy resources into the existing distribution systems. Since the microgrid is a new rising concept, studies on microgrids have been done which use either real hardware test facilities or software simulation testbeds.

In the work presented in this manuscript, a simulation model of a microgrid with renewable energy sources was implemented in PSCAD/EMTDC. The models developed in this work include fundamental power system components, three DER units with control (including a wind energy source, a solar energy source, and an energy storage source component), the protective relays, and other necessary components for a microgrid. The voltage level of the microgrid in this work was rated at 480V for line-to-line and 277V for line-to-ground. Using the microgrid model, simulation case studies were conducted to observe the performance and operational scenarios of the developed microgrid models and system.

This thesis follows the style of *IEEE Transactions on Power Systems.*

1.2. Organization of Thesis

The thesis is organized into 5 sections. Section 1 provides the introduction and overall implementation and research objectives for this work. Section 2 provides the literature review conducted in the areas of microgrid, distributed energy resource unit control and renewable energy sources, and the problem statement. Section 3 provides the details of the PSCAD/EMTDC-based implementation of the microgrid model. Section 4 presents various simulation case studies conducted to demonstrate the different aspects of the microgrid system model that was developed. Finally, Section 5 presents the conclusions and future work.

2. LITERATURE REVIEW AND PROBLEM STATEMENT

2.1. Microgrid Concept

There is a trend that the power distribution systems now served by large power generators will be enhanced with more distributed energy resource (DER) architectures are less restrictive [2]. However, the increasing number of the distributed generation with less restriction can cause as many problems as it may solve. A system approach to view generation and associated loads as a subsystem or a "microgrid" is a better way to realize the emerging potential of distributed generation. The microgrid can be considered as a controllable cell of the power system [3].

Even though there is no universally accepted standard definition for a microgrid, certain characteristics are generally common in the existing microgrids. A microgrid is composed of interconnected distributed energy resources which are capable of providing sufficient and continuous energy to a large percent of the microgrid internal load demand. Also, a microgrid possesses independent controls and intentional islanding takes place with minimal service interruption [4]. For instance, in the CERTS microgrid concept, a microgrid must be able to operate parallel with the grid, and also should have the ability to isolate itself from the utility seamlessly with little or no disruption to the loads within the microgrid during a disturbance [5]. A microgrid should be able to operate in both grid-connected mode and islanded mode (autonomous mode). Many publications present the benefits that microgrids can bring. For example, it can maximize the use of

renewable energy, increase the reliability level, and enhance power quality for local customers' loads [6]. A typical microgrid configuration is shown in Fig. 2.1 [1].

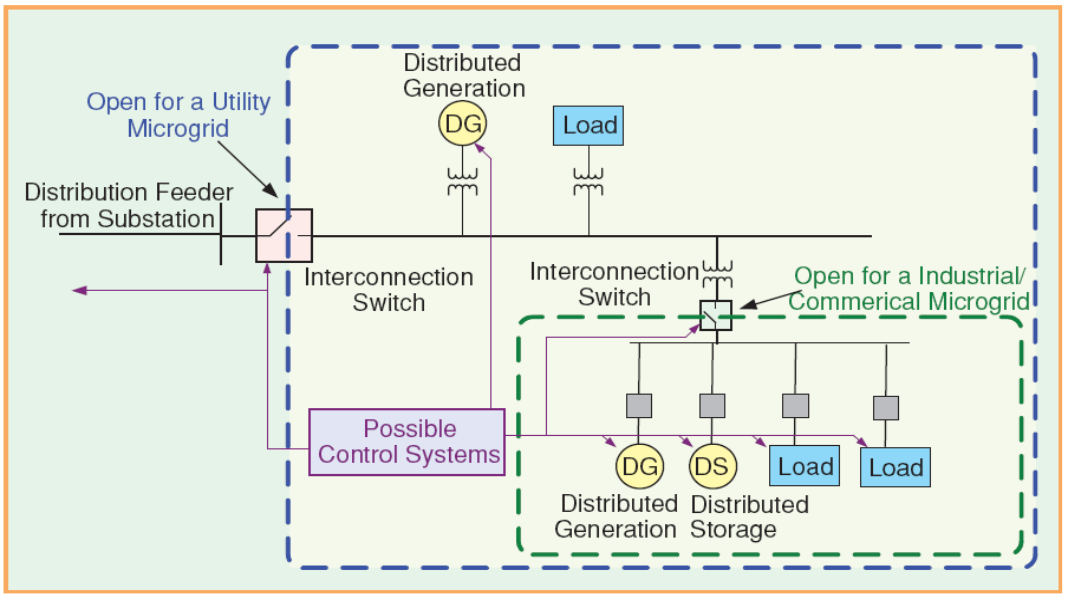

Fig. 2.1. A typical microgrid configuration [1]

2.2. Microgrid Classification

According to the microgrid whitepaper from the U.S. Department of Energy, microgrids can be grouped into a number of different classes based on the control systems as shown in Table 1 [7]. Additional criteria to classify microgrids have been presented in the literature. For example, from microgrid architectures and their characteristics based on applications, ownership structure, and type of loads served,

microgrids can be classified into three categories: utility microgrids, commercial and industrial microgrids, and remote microgrids [8].

Table 1 Microgrid characteristics for different classes [7]

<table>
<tr><td></td><td>Simple (class I)</td><td>Master Control (class II)</td><td>Peer-to-Peer Control (Class III)</td></tr>
<tr><td rowspan="2">Specific Microgrid Characteristics for different classes</td><td>Generators located in central power plant</td><td>Generators distributed in separate buses</td><td rowspan="2">No master control exists.
Local control at each generator's location maintaining voltage and frequency stability.</td></tr>
<tr><td colspan="2">Master control system to both meet the loads and provide voltage and frequency support to the microgrid.</td></tr>
<tr><td>Common Microgrid Characteristics</td><td colspan="3">o Multiple generators serving loads in multiple locations
o The generators and facilities are connected by a distribution grid which is interconnected with utility-owned area electrical power system
o Event detection and response control</td></tr>
</table>

2.3. Control of Distributed Energy Resources Units

Distributed energy resources (DERs) are the key components in microgrid systems. DERs are small-scale power generation or storage technologies that are located close to the load they serve. The typical range of the DERs is between 3kW to 10kW. The small-scale power generation is called distributed generation (DG), and the small-scale storage is called distributed storage (DS). They are used to provide an alternative to or enhancement of the traditional electric power systems, etc. [9]. DERs may refer to the devices and technologies including combined heat power, fuel cells, microturbines, photovoltaic systems, small wind power systems, etc. They play essential roles in the microgrids. Power electronics technologies, such as rectifiers, inverters and DC to DC converters are involved to integrate DERs into microgrid systems.

Control strategies for DER units within a microgrid should be selected based on the required functions and possible operational scenarios. The main control functions for a DER unit are voltage/frequency control (V/F control) and active/reactive power control (PQ control). A general categorization of the major control methods of a DER unit is shown in Table 2 [10].

Table 2 Classification of control strategies for electronically coupled DER units [10]

Control Method	Grid-Following Controls	Grid-Forming Controls
Noninteractive	Power export with/without maximum power point tracking (MPPT)	Voltage and frequency control
Interactive	Power dispatch Real and reactive power support	Load sharing (droop control)

In Table 2, grid-following control means the voltage and frequency of a DER unit follow those of the utility grid or other sources, thus it is mainly applied in grid-connected mode. In contrast, grid-forming control means a DER unit itself determines the voltage and frequency in islanded mode. Each of the two ways can be classified into noninteractive control and interactive control. The term "interactive" means the output power of DER unit depends on the conditions of other units or loads.

Local frequency control is always one of the main issues when a microgrid operates in islanded mode. The reason is that an electronically coupled DG unit does not exhibit any inertia during the microgrid transients and thus has no capability to maintain the microgrid frequency [10]. When a microgrid transfers from grid-connected mode to islanded mode, the DG units in the microgrid need to maintain the frequency.

The Grid-Forming control strategy emulates behavior of a "swing source" in an islanded microgrid [10]. The reason is when the microgrid transfers from grid-connected

mode to islanded mode, the power balance between supply and demand do not match at the moment. Due to the low inertia of the system, the system frequency may fluctuate [11]. The grid-forming strategy as a “swing source” picks up the unbalanced load and maintains the system frequency in a tight range.

If only one DER unit is in the system, it can be assigned to regulate the voltage at the interconnecting point and dominantly set the system frequency. When two or more DER units exist in a microgrid, the droop control technique is one technique that is commonly used [10]. Droop control technique is a method to achieve the peer-to-peer control as mentioned in Table 1. The droop control technique includes frequency-droop (f-P droop) and voltage-droop (v-Q droop). This technique is a way to make the inverters in the microgrid system to perform a load sharing function in islanded mode. The droop control technique was first developed for inverter parallel operations [12]. It has been widely used in many microgrid cases. A typical microgrid with droop control techniques is the CERTS microgrid testbed facilities. In the CERTS microgrid, the three DGs use the droop control technique to control the voltage and frequency levels in islanded mode operation [5]. As shown in Table 2, in this class of microgrids, interactive control is used for the DER units.

According to Table 1, besides the peer-to-peer control, another class of microgrids uses master control method. In the master control class microgird, the droop control technique is not necessarily applied in DER units. When the microgrid transfers from grid-connected mode to islanded mode and there is no droop control to perform load sharing functions to pick up the unbalanced load, a “swing source” with enough

reserved energy is used. This “swing source” performs function of load sharing and maintains the system voltage and frequency. Obviously, in this situation, some energy storage source (ESS) must be included in the microgrid system to balance the load requirement. The ESS plays an important role to maintain the system frequency and voltage in this type of microgrid. A typical example of this class of microgrids is the hardware-in-loop simulation system (HILS) for micrgorid management system developed by Korea Electrotechnology Research Institute using RTDS [11]. In this class of microgrids, the DER units use noninteractive control, as shown in Table 2, when they operate in islanded mode to enable grid-forming control.

2.4. Microgrid Testbed Facilities

Microgrid testbed facilities or test sites have been built in different locations such as in the United States, Japan, Canada, and Europe [1]. For example, the microgrid developed by the Consortium for Electric Reliability Technology Solutions (CERTS) in the United States is a test site based on the class III microgrid concept. The renewable energy sources have not been installed into it as of yet [13]. The Aichi microgrid project in Japan utilizes renewable energy sources, battery storage, and also the capability for heat supply [14]. In the European Union (EU) microgrid projects, a couple of test sites with different topologies have been built up [15]. The microgrid system implemented in the Remote Islands in the Republic of Maldives has incorporated wind, PV and diesel energy sources together [16]. These three microgrid example are based on class II microgrid concept. Besides the physical facilities, software simulation systems for microgrids have also been developed, such as the RTDS model of a test microgrid

developed by Korea Electrotechnology Research Institute (KERI) as previously mentioned [11].

2.5. Wind Energy Sources

Renewable energy is energy generated from natural resources which are renewable (naturally replenished) such as sunlight, wind, rain, tides and geothermal heat, [17]. Renewable energy sources (RESs) such as wind turbine and photovoltaic systems are favored for DERs for their advantages, such as low maintenance and low pollution. In recent decades, wind energy has become increasingly important throughout the world. Through wind turbines, wind energy is converted into electrical energy. For a typical three blades horizontal axis MOD-2 wind turbine, the blade dynamics are approximated by the equations (1) – (3) [18],

$$\gamma = \frac{V_W}{\omega_B} \tag{1}$$

$$C_P = \frac{1}{2}(\gamma - 0.022\beta^2 - 5.6)e^{-0.17\gamma} \tag{2}$$

$$P_W = \frac{1}{2}\rho A C_P V_W^3 = \frac{1}{2}\rho A \omega_{BO} C_P \gamma V_W^2 \tag{3}$$

where

$P_W = Output\ power\ of\ wind\ turbine\ [W]$

$V_W = wind\ velocity\ [mi/h]$

$\omega_B = blade\ angular\ velocity\ [mech\ rad/s]$

$\gamma = tip\ speed\ ratio\ [(mi-h)/(rad/s)]$

$\beta = blade\ pitch\ angle\ [degrees]$

$C_P = power\ coefficient\ (dimensionless)$

$$\rho = air\ density\ [lbf/ft^3]$$

$$A = blade\ impact\ area\ [ft^2]$$

Another way to define tip speed ratio (TSR) as λ instead of γ is shown in equation (4) [19],

$$\lambda = \frac{R}{\gamma} \tag{4}$$

where

$$R = blade\ radius$$

The tip speed ratio λ for wind turbines is the ratio between the rotational linear speed of the tip of a blade and the actual velocity of the wind. γ is the ratio between the actual velocity of the wind and the rotational angular speed of the tip of a blade.

The wind turbine characteristic is shown in Fig. 2.2 [20]. The first figure shows the curve of the power coefficient versus tip ratio. The second figure shows the curves for the relationship between the output power and the rotor speed.

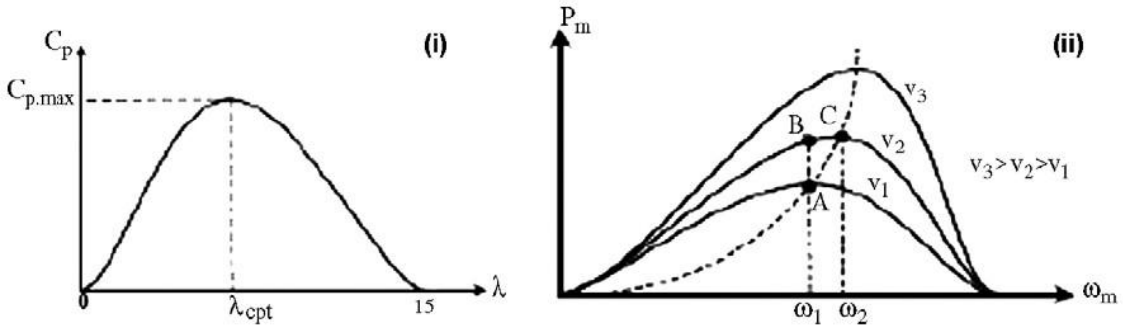

Fig. 2.2. (i) Power coefficient vs. tip ratio and (ii) output power vs. rotor speed for three different wind speeds

Due to the fast development on technologies both for generators and for power electronics, the wind turbines mix and match many innovative concepts with the proven technologies. Four types of configurations for wind energy sources are shown in Fig. 2.3 [21]. In this figure, SCIG = squirrel cage induction generator; WRIG = wound rotor induction generator; PMSG = permanent magnet synchronous generator; WRSG = wound rotor synchronous generator. Each of the configurations above has its own specifics which will be introduced in the following paragraphs [21].

Type A is a fixed speed wind-turbine with an induction generator. Type B corresponds to a limited variable speed wind turbine with variable generator rotor resistance. Type C is known as doubly fed induction generator (DFIG), where the wind turbine with limited variable speed is connected with a partial scale frequency converter. All of these three types are not able to work independently in an islanded mode. The reason is that an induction generator has to receive its exciting current from another source and consumes reactive power. Reactive power may be supplied by the grid or by

a power electronic system. The generator's magnetic field is established only if it is connected to the grid or another source. When a microgrid transfers from grid-connected mode into islanded mode, lack of excitation current from the external sources may lead to the induction generator not working. Thus when one of these types of configurations for a wind turbine is used, it usually comes with other DG units. An example is the microgrid system in M. Shahabi et al.'s work [22], where a doubly fed induction wind generator works together with a gas-turbine synchronous generator in the islanded mode.

Type D is a synchronous generator together with a full scale frequency converter. Compared to the previous three types, type D has two advantages: first, its rotor speed can change in a large range thus it has the capability for variable speed control, which makes the maximum power point tracking function possible; second, it can use an excitation system which is independent from the grid or other sources so that it can operate alone without other external provided excitation. An example of this configuration applied into microgrid is the work done by KPRI [11] .

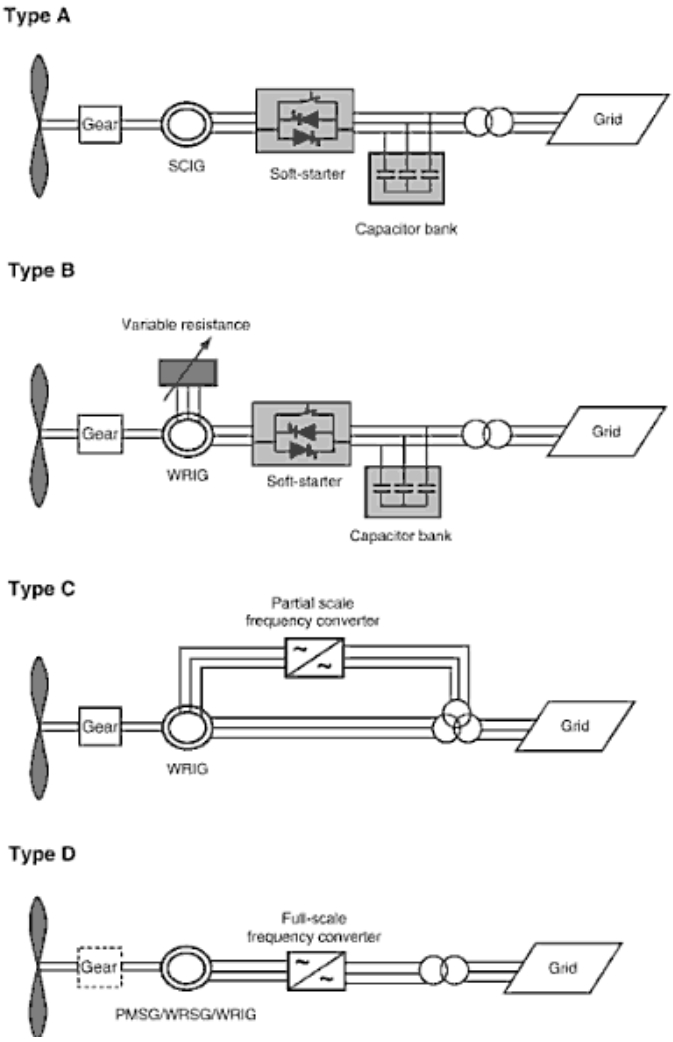

Fig. 2.3. Typical wind energy source configurations [21]

2.6. Solar Energy Sources

Solar energy refers to energy that is collected from sunlight. By the photovoltaic effect, the energy from the sunlight can be directly converted into electricity by using a photovoltaic cell (PV cell). Besides the wind energy source, solar energy source with PV

cells is another favored source as distributed generation. PV arrays as the DER units are used in the microgrids in Japan, Maldives and Europe [14] [15] [16].

A simplified equivalent circuit model which represents the electrical behavior of the actual cell module is shown in Fig. 2.4 [23]. The output current of a PV module can be obtained from equation (5),

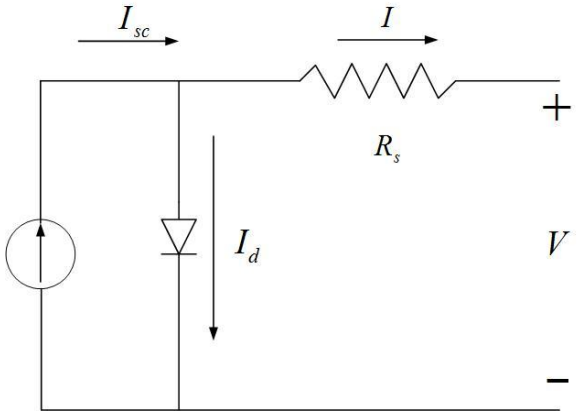

Fig. 2.4. Equivalent circuit of a PV module

$$I = I_{sc} - I_d = I_{sc} - I_0[\exp\left(\frac{V+IR_s}{nV_T}\right) - 1] \tag{5}$$

where

$I = output\ current\ of\ PV\ module\ [A]$

$I_d = diode\ current\ [A]$

$I_{sc} = short\ cicuit\ current\ of\ PV\ module\ [A]$

$I_0 = diode\ saturation\ current\ [A]$

$V = terminal\ voltage\ of\ PV\ module\ [V]$

$R_s = series\ resistance\ [\Omega]$

$n = ideal\ constant\ of\ diode\ (1{\sim}2)$

$V_T = thermal\ potential\ of\ PV\ module\ [V]$

A typical PV module characteristic is shown in Fig. 2.5 [20]. The first figure shows the curves of the output current versus output voltage of a PV module. The second figure shows the relationship between the output power and the output voltage of a PV module.

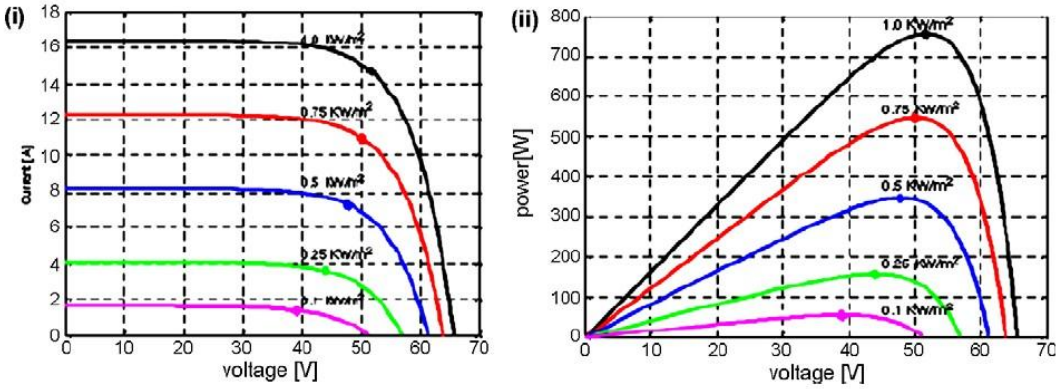

Fig. 2.5. (i) I-V characteristics of a PV module and (ii) P-V characteristics of a PV module

Usually a PV array consists of a group of PV modules for obtaining high power. Those modules in a PV array are connected in series-parallel combinations. The output current of a PV array can be obtained from equation (6),

$$I = N_p I_{sc} - N_p I_0[\exp\left(\frac{V+IR_s}{nN_S V_T}\right) - 1] \quad (6)$$

where

$$N_p = number\ of\ parallel\ PV\ modules\ in\ a\ PV\ array$$

$$N_s = number\ of\ series\ PV\ modules\ in\ a\ PV\ array$$

The current versus voltage and power versus voltage characteristics of a PV array are similar as the characteristics of a single module shown in Fig. 2.5.

A PV array usually connects with a DC/DC converter, which is used to step up the output voltage of the PV array. Through the control of the DC/DC converter, some advanced technique could be used for a PV array, such as the maximum power point tracking (MPPT) function. In order to connect a PV array in an AC grid system, an inverter should be used to convert the DC output of a PV array into AC output.

2.7. Problem Statement

Since the microgrid is a new rising concept, studies on microgrids are being performed which require either hardware test facilities or software simulation testbeds. Implementing a microgrid simulation model with renewable energy source models enables us to do further studies and research on microgrids.

PSCAD, also known as PSCAD/EMTDC [24] is a powerful electromagnetic time domain transient simulation environment and study tool. It is widely used in power system simulations, including systems with DER units. Therefore PSCAD/EMTDC is used for the proposed microgrid system model and simulation in this work.

The implementation of the simulation model of the proposed microgrid system in PSCAD includes several parts: 1) develop the fundamental power system component models; 2) develop the DER unit models and their controller including wind energy, solar energy and energy storage sources; 3) integrate the individual component models into the system and develop the protection scheme and component models.

Based on the microgrid system model in PSCAD, case studies were conducted to observe the performance and operational scenarios of the microgrid models and systems.

3. MICROGRID SYSTEM MODEL

3.1. Introduction

To implement a microgrid system, the initial step is to determine the microgrid structure and topology. The CERTS microgrid basic structure and topology were chosen and a portion of components were used in this work. The reason is that the CERTS microgrid is one of existing sites with the most publications and information available. The main differences between the CERTS microgrid reported and the proposed microgrid model in this work are as following: First, the CERTS microgrid only contains diesel generators, but in the proposed microgrid system reported in this thesis, wind, PV and energy storage units are included. Second, the CERTS microgrid applied droop control to each source, which is class III microgrid as presented in Section 2. The microgrid modeled in this work applied PQ control and voltage source inverter control for different sources, which is a class II microgrid. Even though its DER unit control method is different from the proposed method in this work, the rating level, basic components, and protection scheme can still be used after proper modification.

A one-line diagram of the proposed system modified from the CERTS microgrid is shown in Fig. 3.1. The system is divided into six zones. Zone 3, Zone 4 and Zone 5 are defined as critical loads zones. Each of them has one DER unit, one 75 yard cable, one transformer, and one load bank (including resistive load and inductance load). Zone 6 is defined as a noncritical load zone, which includes one 75 yard cable and one load

bank. Additionally, each of these zones has a point to connect a possible fault load. The electrical nodes are marked in the system. Cables are used to connect the neighboring nodes. The interconnection switch is the point which connects the microgrid with the utility grid. The load in Zone 6 is not considered to be a part of the microgrid.

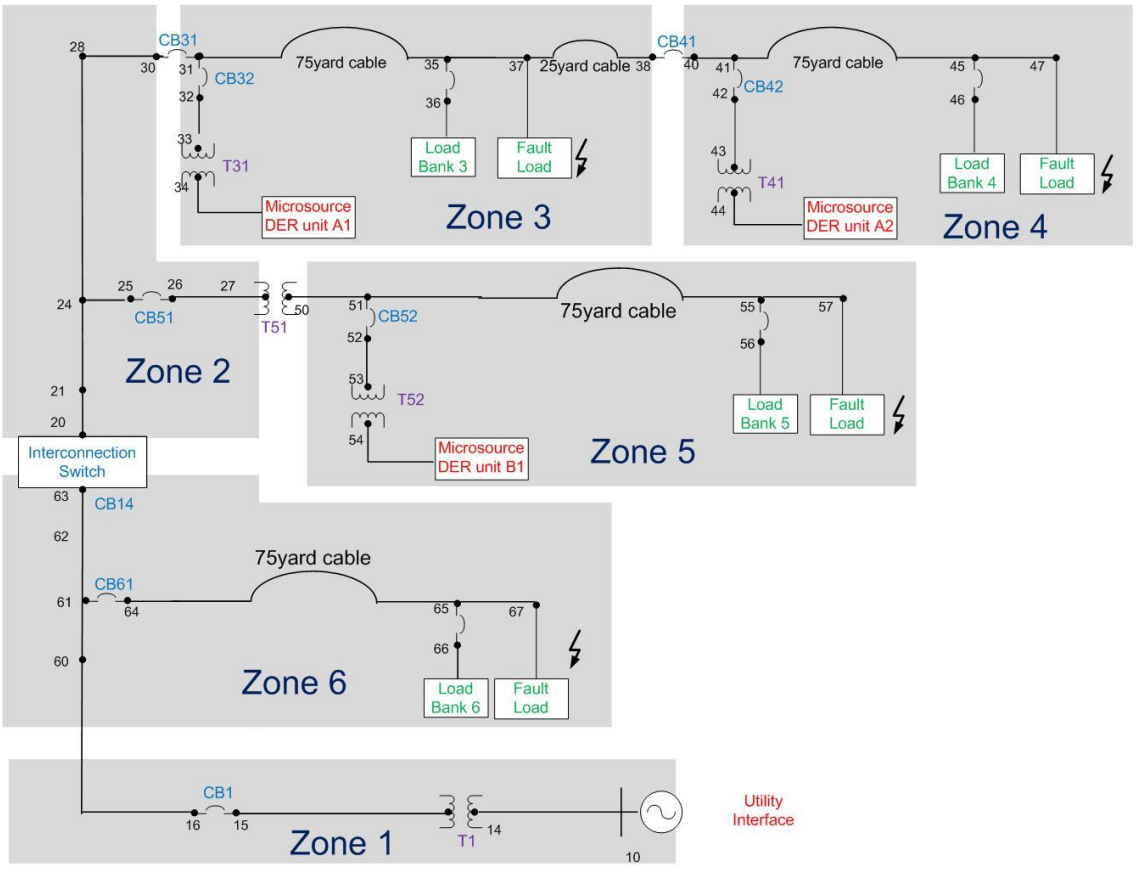

Fig. 3.1. The structure and topology of the proposed microgrid system

The implementation process includes modeling all of the necessary component models of the microgrid system. Some of the component models exist in the PSCAD library. The parameters needed in PSCAD were specified based on the functions and ratings for each of these components. Some other component models are not directly available in the PSCAD library, thus they were developed in PSCAD.

3.2. Fundamental Power System Component Models

Fundamental power system components refer to the basic components in a distribution system besides the DER units and protection relay. The basic components consist of transformers, cables, resistive loads, inductive loads, motors, etc. Most of these component models exist in the PSCAD library. The functions, ratings, and parameters for each component in PSCAD were determined. For example, as presented in Fig. 3.1, six transformers are used in the proposed microgrid system. The data are shown in Table 3.

Table 3 Transformers summary

Transformer	Primary Voltage(V)	Secondary Voltage(V)	Rating(kVA)	X/R	Z%
T11	480	480	500	6	5
T31	480	480	112.5	5	1
T41	480	480	112.5	5	1
T51	480	480	112.5	5	1
T52	480	480	112.5	5	1

An ideal AC source was used for modeling the utility grid. The utility grid's line to line RMS voltage level was 480V. The utility interface was modeled as a three-phase, 480V/60Hz AC voltage source, with no inner resistance. Thus an ideal source with resistance 0 Ω was used.

The resistive and the inductive load model in the original reference microgrid testbed are shown in Fig. 3.2 and Fig. 3.3, respectively [13]. Each of the resistive load banks contains one 5kW, one 10kW and four 20kW resistive loads. All of these loads are three-phase, with switches in branches of each phase. The resistive load bank can vary from 0kW to 95kW with single phase or three phases connected. In this work, a combination of constant resistive loads was used to represent the resistive load bank in PSCAD. The inductive load banks were modeled in a similar way as the resistive load bank. The inductive loads can vary from 0kVar to 60kVar with a single phase or three phases connection.

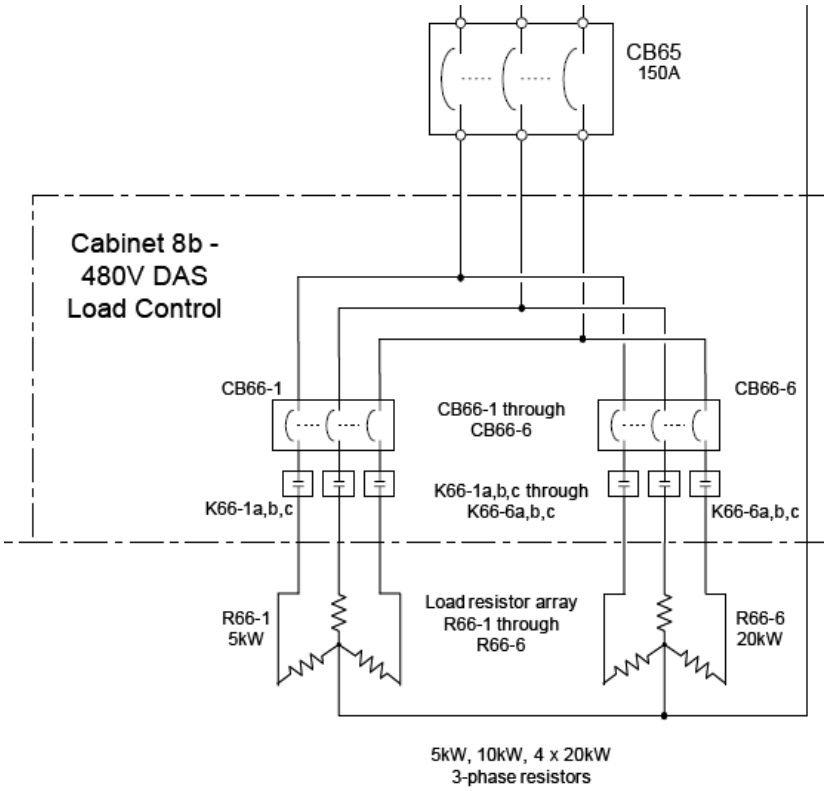

Fig. 3.2. Resistive load model in the original schematic [13]

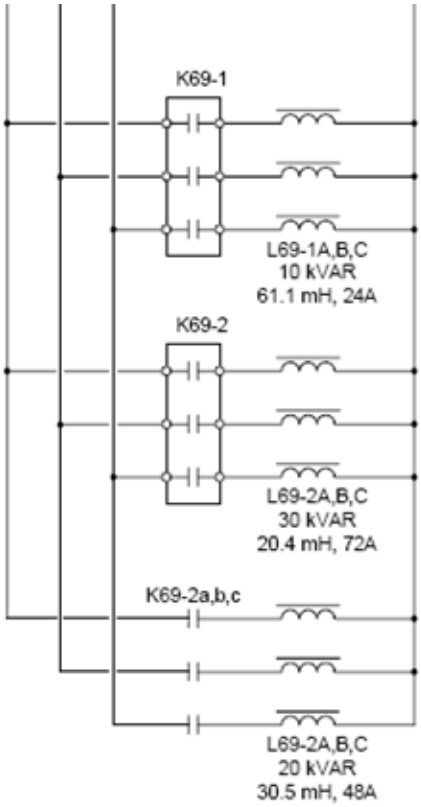

Fig. 3.3. Inductance load model in the original schematic [13]

Cable models are necessary to connect the neighboring electrical nodes in the proposed system. Assumptions were made for the cables used in the proposed system as shown in Table 4. Due to the nodes limitation in the PSCAD version for this work, some cables were neglected. Only five long cables with length information in Fig. 3.1 were used to represent the distance between different zones. All of the cables were modeled in PSCAD/EMTDC as π section models, where the cable parameters are represented by an equivalent circuit composed by resistance, inductance and capacitance.

Table 4 Cables information

Cable Section Number	1	2	3	4	5
From (node number)	64	31	36	41	51
To (node number)	65	35	37	45	55
Location	Zone6	Zone3	Zone3	Zone4	Zone5
Maximum Load Real power (kW)	180	290	180	180	180
Maximum Load Reactive power (kVar)	60	120	60	60	60
Maximum Current per phase (A)	228.5	377.7	228.5	228.5	228.5
Rating Line to Line Voltage (V)	480	480	480	480	480
Length (m)	68.58	68.58	22.86	68.58	68.58
Neutral	Yes	Yes	Yes	Yes	No
Size (AWG or kcmil)	AWG 2	AWG 2/0	AWG 2	AWG 2	AWG 2

3.3. Wind Energy Source Model

3.3.1. Introduction of the Wind Energy Source Model

In the microgrid system, a wind energy source model was designed. As discussed in the literature review section, there are four main types of configurations for wind turbine operation. After comparing these configurations, the variable speed wind turbine with a synchronous machine was chosen for this model. This configuration has the advantages of full variable-speed control maximum power point tracking (MPPT) capabilities with proper control method [21], [25]. The configuration is shown in Fig. 3.4. Wind energy source model includes four main parts: wind turbine, synchronous generator, rectifier and inverter. The wind turbine output torque serve as the input torque of the synchronous generator. The three phase output voltages of the synchronous

generator are input to the rectifier. A capacitor serves as a DC link between the rectifier and the inverter.

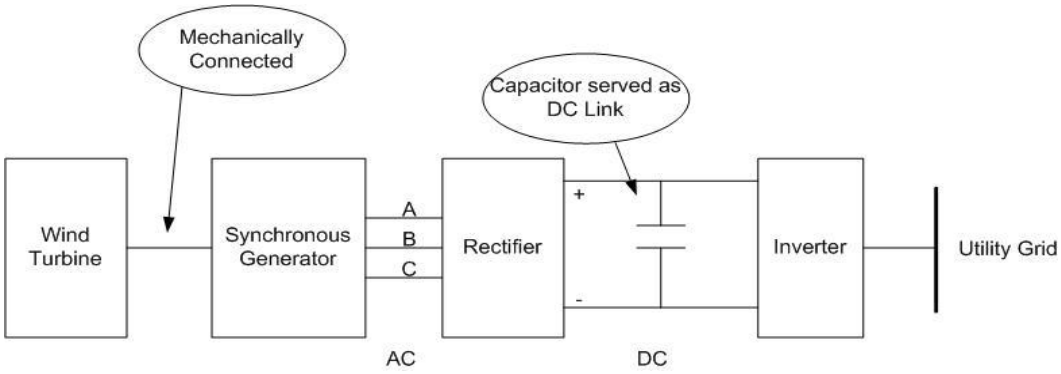

Fig. 3.4. The wind energy source configuration

Among these parts, the wind turbine component and synchronous generator component are available in the PSCAD library directly. The model in the PSCAD library was used with proper parameters based on the ratings. The rectifier and inverter models are not available in PSCAD, so they were developed in this work.

3.3.2. Wind Turbine Model

Three models related to wind energy are available in the PSCAD library as shown in Fig. 3.5, including the wind source model, wind turbine model and wind governor model. In this work, the wind source model and the wind turbine model were used.

In PSCAD, the wind source model generates the wind speed variable. The wind speed variable can be composed by four components as shown in equation (6) [18]. The values of those four components can be independently set when necessary.

$$V_{Wind} = V_{base} + V_{gust} + V_{ramp} + V_{noise} \tag{6}$$

Where

$V_{base} = base\ wind\ speed\ [m/s]$

$V_{gust} = gust\ wind\ component\ [m/s]$

$V_{ramp} = ramp\ wind\ component\ [m/s]$

$V_{noise} = noise\ wind\ component\ [m/s]$

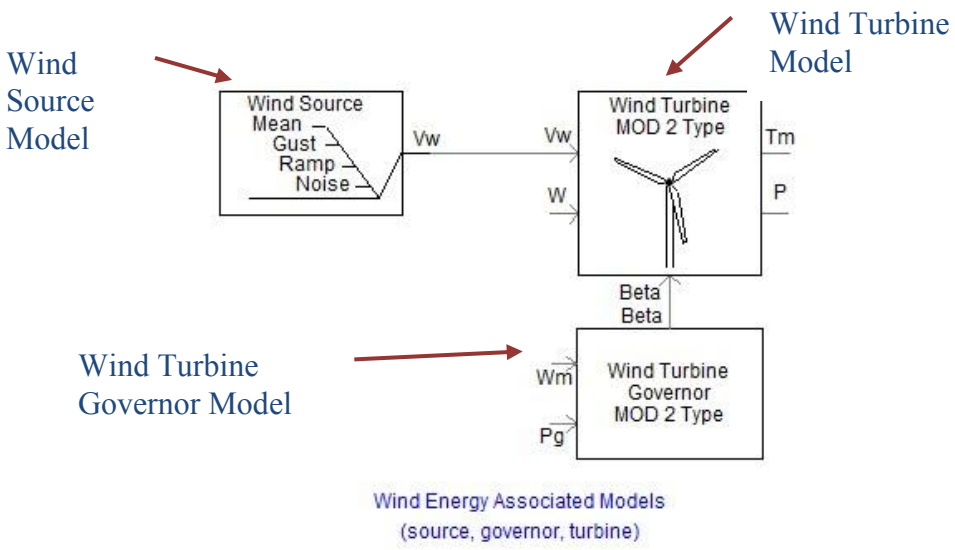

Fig. 3.5. Components in PSCAD library related to wind energy

As previously mentioned, the wind turbine model produces the output torque T_m. It follows the turbine equation (1) – (4). The low frequency mechanical dynamic effects of a wind turbine such as tower shadow and wind shear effects were not taken into consideration. In the microgrid system, the parameters for the wind turbine were set as shown in Table 5. The gear ratio was set to be 1 to model a gearless turbine, thus the wind turbine rotor speed would be the same as the synchronous generator mechanical speed. A given wind speed, a rotor speed and the parameters in Table 5 determine the output mechanical torque T_m . T_m is then fed into the connected synchronous machine.

Table 5 Wind turbine parameters

	Value	Unit
Generator Rated MVA	0.15	MVA
Machine rated angular mechanical speed	0.4	Hz
Rotor Radius	10	m
Rotor Area	314	m^2
Gear Ratio	1	
Gear Box Efficiency	1	pu
Equation for power coefficient	MOD2	

The wind turbine governor in the PSCAD library is designed for enabling the pitch control function when necessary. It output pitch angle value as "Beta" shown in Fig. 3.5. However, this component was not used in this work since the pitch angle control scheme was not used. A constant value was given as the pitch angle for the wind turbine.

The relationship between the output power and rotor speed of the wind turbine in this work, for different wind speeds, is shown in Fig. 3.6. The five curves represent the wind turbine characteristic when the wind speed is 5m/s, 7m/s, 10m/s, 12 m/s, and 15 m/s, respectively.

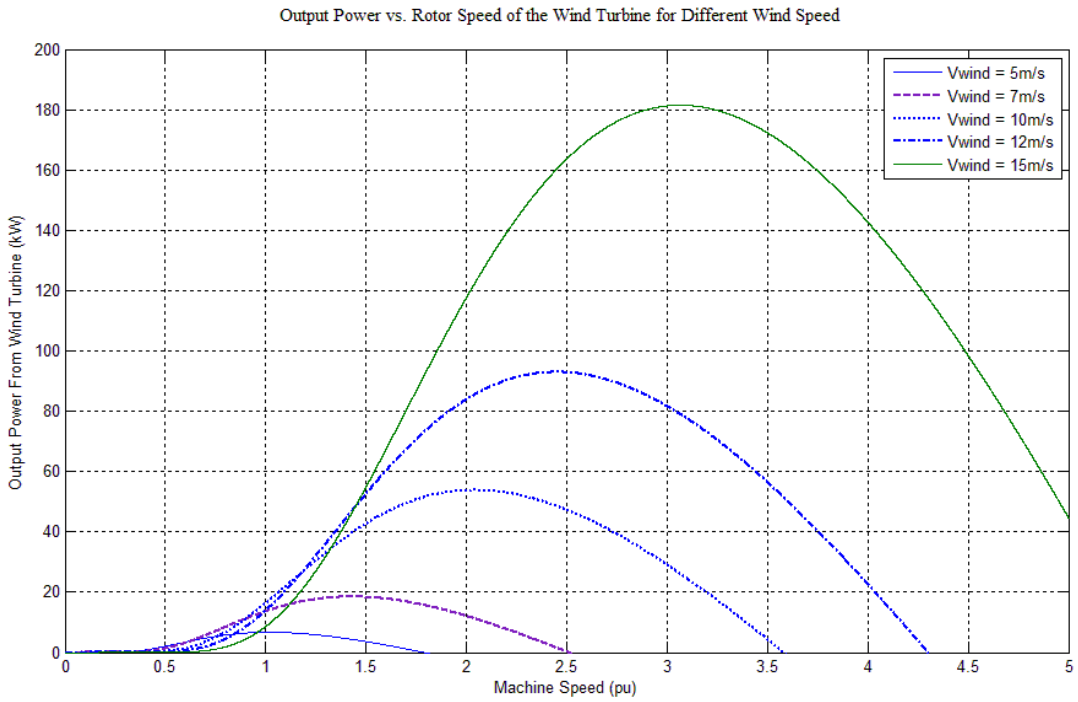

Fig. 3.6. Output power vs. rotor speed for different wind speeds of the wind turbine

3.3.3. Synchronous Generator Parameters

The synchronous generator model and the related exciter are directly available in the PSCAD library. Based on the ratings of the 0.15MW wind turbine, a synchronous generator with the same power rating was chosen. The pole pairs number was set to be 150. The parameters of the synchronous generator were specified as shown in Table 6. Those parameters were obtained from linear extrapolation of two distributed synchronous generator with pre-known parameters. The exciter component for a synchronous machine is also directly available in PSCAD library. The IEEE type AC1A

exciter model and a group of typical data for it from [26] were used. Some parameters were used as the default values provided in PSCAD.

Table 6 Synchronous generator parameters

Category	Parameters	Value	Unit
Basic Data	Rated RMS Line-to-Neutral Voltage	0.48	kV
	Rated RMS Line Current	0.1042	kA
	Base Angular Frequency	60	Hz
	Inertia Constant	0.413	s
	Mechanical Friction and Windage	0.01	pu
	Neutral Series Resistance	20	pu
	Neutral Series Reactance	0	pu
	Iron Loss Resistance	80	pu
Generator Data Format	Armature Time Constant [Ta]	0.332	s
	Potier Reactance [Xp]	0.130	pu
	D: Unsaturated Reactance [Xd]	2.55	pu
	D: Unsaturated Transient Reactance [Xd`]	0.229	pu
	D: Unsat. Transient Time (Open) [Tdo`]	0.011	s
	D: Unsat. Sub-Trans. Reactance[Xd``]	0.222	pu
	D: Unsat. Sub-Trans. Time (Open) [Tdo``]	0.035	s
	Q: Unsaturated Reactance [Xq]	1.17	pu
	Q: Unsaturated Reactance [Xq``]]	0.289	Pu
	Q: Unsa. Sub-Trans. Time (Open) [Tqo``]	0.010	s
	Air Gap Factor	1.0	
Initial Conditions	Terminal Voltage Magntitude at Time = 0-	1.05	pu
	Terminal Voltage Phase at Time = 0-	0.406	rad
Initial Conditions if Starting as a Source	Time to Ramp Source Limit to Rated	0.1	s

3.3.4. Frequency Converter

A frequency converter is composed of a rectifier, a DC link capacitor, and an inverter. The output power of the frequency converter can be controlled through the proper method [25] [27]. Part of the method developed by S. K. Kim et al was applied in the microgrid system. The circuit model of the frequency converter is shown in Fig. 3.7. The output electrical nodes of the synchronous generator are connected into a diode bridge rectifier. The inductance L serves as a filter. A capacitor is in parallel with the output of the rectifier to serve as a DC link. The DC capacitor was set to be 50mF, which is a proper value to obtain a good performance. A much smaller or much larger capacitor could lead stability problem. During a transient, when the output power of the synchronous generator is more than the required power of the inverter, the extra energy could be absorbed into the capacitor and lead the DC link voltage to increase.

The inverter is connected after the inductance L and the paralleling DC link capacitor. The pulse-width modulation (PWM) technique has been applied for the inverter control. The inverter uses the PQ control mode which allows the output power to be a constant value. The control scheme is shown in Fig. 3.8.

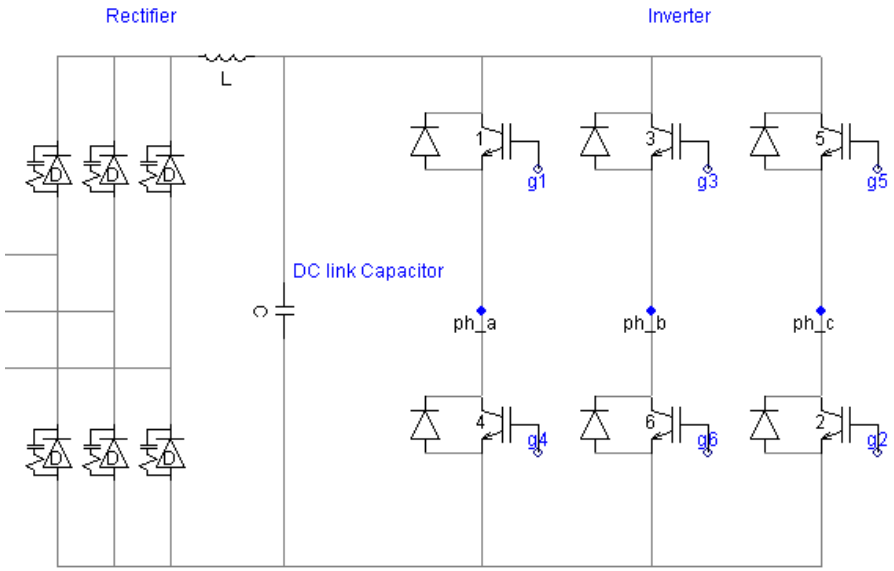

Fig. 3.7. The frequency converter modeled in PSCAD

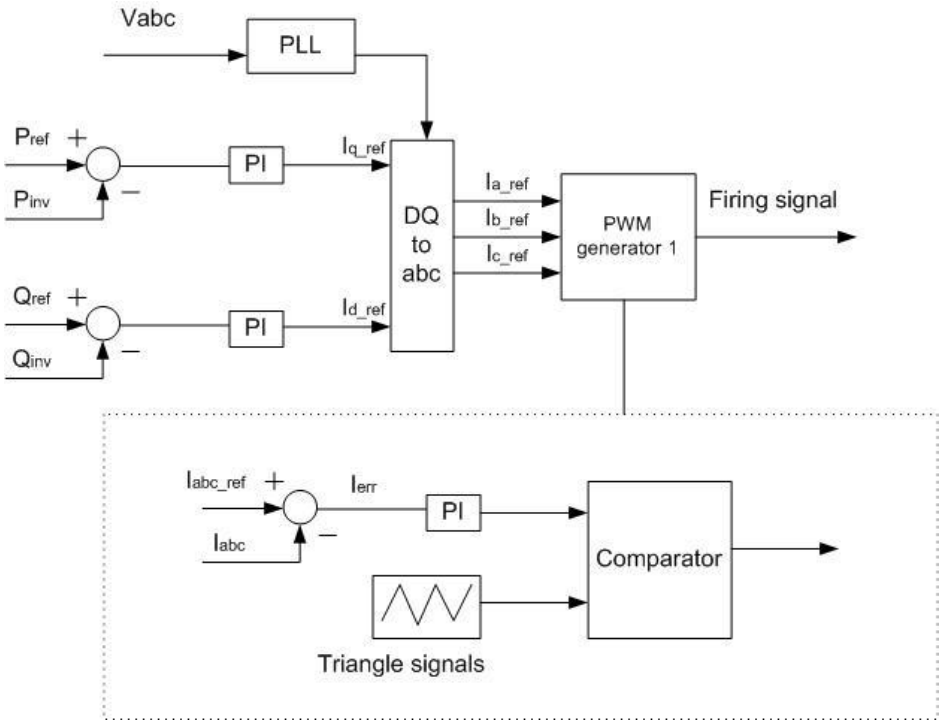

Fig. 3.8. The current control scheme in the PQ control mode

As shown in Fig. 3.8, in the PQ control mode of the inverter, the real power reference P_{ref} and reactive power reference Q_{ref} are set as the prerequisite reference values. The errors between power references P_{ref} and Q_{ref} and the measured power values P_{inv} and Q_{inv} are processed through PI controllers. From the output values of the PI controllers, the references of q-axis current I_{q_ref} and d-axis current I_{d_ref} can be obtained. Then I_{q_ref} and I_{d_ref} are transformed into abc phase current reference I_{a_ref}, I_{b_ref}, and I_{c_ref}. In a current controller, the current references are compared with the measured current values. These current errors are sent to another PI controller to generate the reference signals of the three phase voltages V_{a_ref}, V_{b_ref}, and V_{c_ref}. The phase-lock-loop (PLL) generates a signal synchronized in phase to the converter input voltage V_{abc} to provide the reference phase angle for the rotational inverse dq transformation. Then the PWM technique is applied to create the switching signals for the six Insulated Gate Bipolar Transistor (IGBT) switches. The six IGBTs g1, g2, g3, g4, g5, and g6 are controlled to turn on or turn off so that the inverter is able to output required AC voltage and current based on the power reference.

An LC filter is connected at the output end of the frequency converter to improve the output power waveforms.

3.4. Solar Energy Source Model

As presented in literature review section, energy from PV cells is another favored resource as distributed generation. As shown in Fig. 3.9, PV energy source model

includes three parts. PV array module and the DC/DC converter were developed by A. Rajapakse in University of Manitoba [28], the parameters were slightly modified for this curve. In this model, the module developed by A. Rajapakse is used as shown in Fig. 3.10. Two PV modules are connected in series and then a large capacitor is connected in parallel with them to serve as energy buffer for the transient. The part is the same one used in the wind energy source model. The parameters of the PV array module are shown in Table 7.

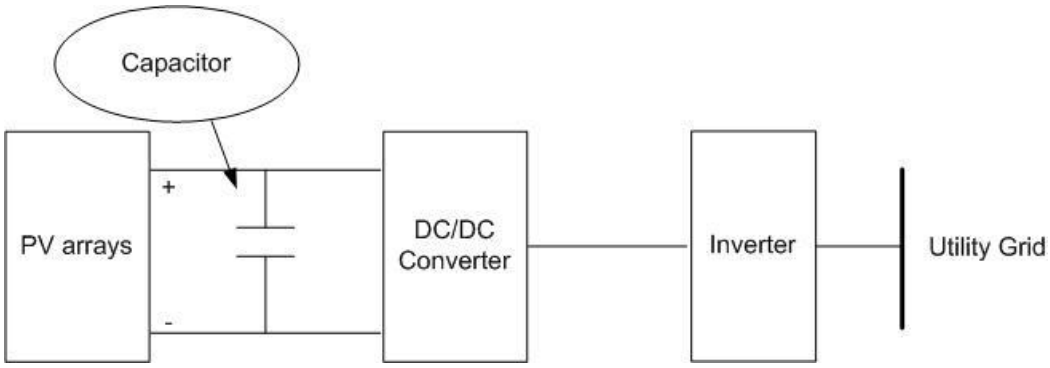

Fig. 3.9. The solar energy source configuration

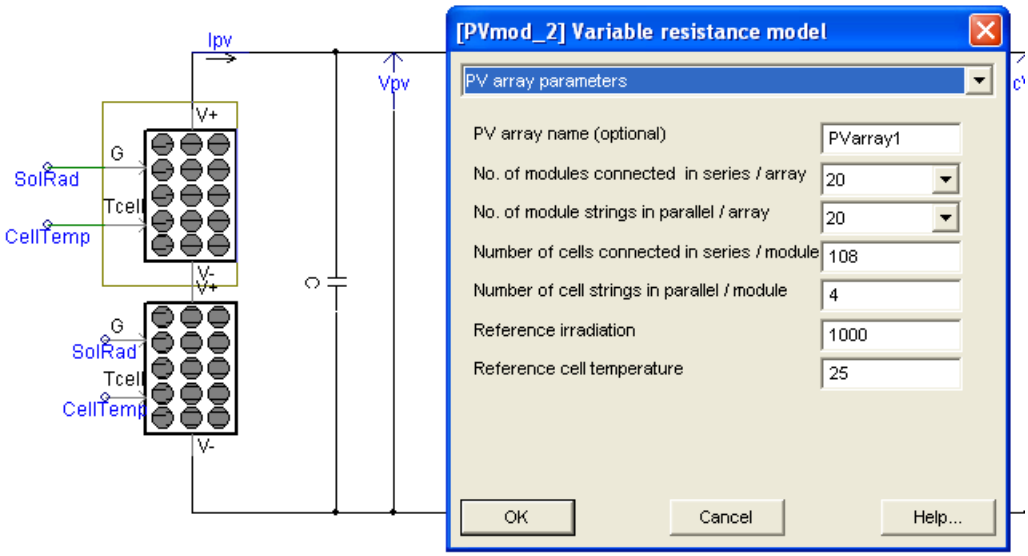

Fig. 3.10. Model of PV arrays and the parameters setting dialogue in PSCAD

Table 7 PV arrays parameters

	Suggested values
Number of modules connected in series/array	20
Number of module strings in parallel/array	20
Number of cells connected in series/module	108
Number of cells in parallel/module	4
Reference irradiation (W/m^2)	1000
Reference cell temperature (℃)	25
Effective area/cell	0.01
Series resistance/cell (Ω)	0.02
Shunt resistance/cell	1000
Diode ideality factor	1.5
Band gap energy (eV)	1.103
Saturation current at ref. conditions/cell (A)	1e-9
Short circuit current at ref. conditions/cell (A)	2.5
Temp. coeff. of photo current	0.001

The relationship between the output current and output voltage for the PV arrays in this work is shown in Fig. 3.11. The curves show the relationship between the voltage and the output power in Fig. 3.12. The five curves in each figure represent the PV module characteristics when the solar radiation is 100 W/m^2, 250 W/m^2 , 500 W/m^2 , 750 W/m^2, and 1000 W/m^2, respectively.

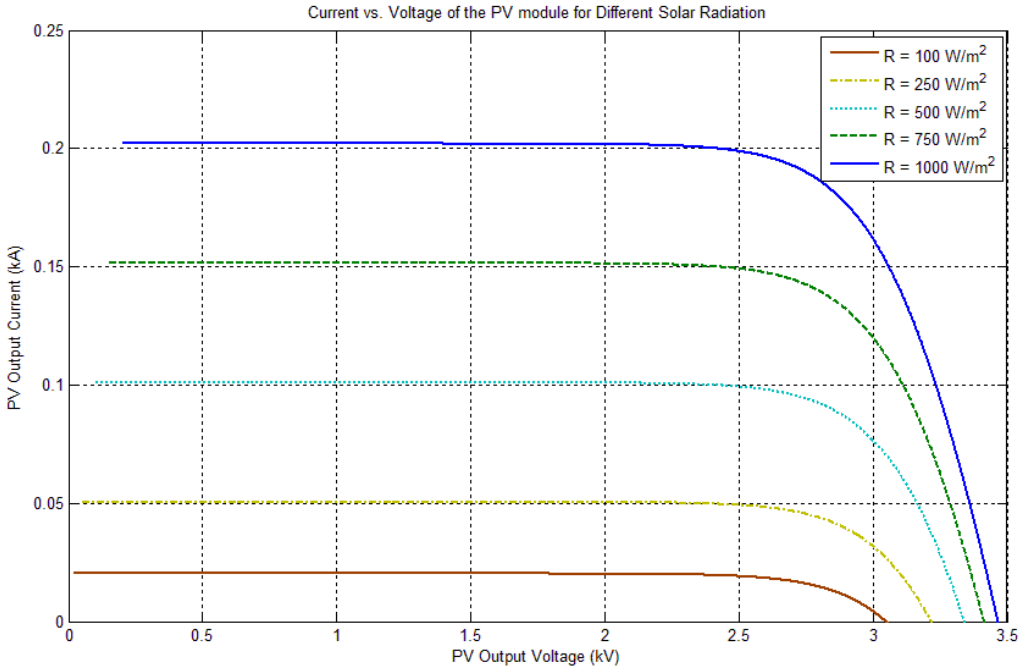

Fig. 3.11. Output current vs. voltage for different solar radiation of the PV arrays

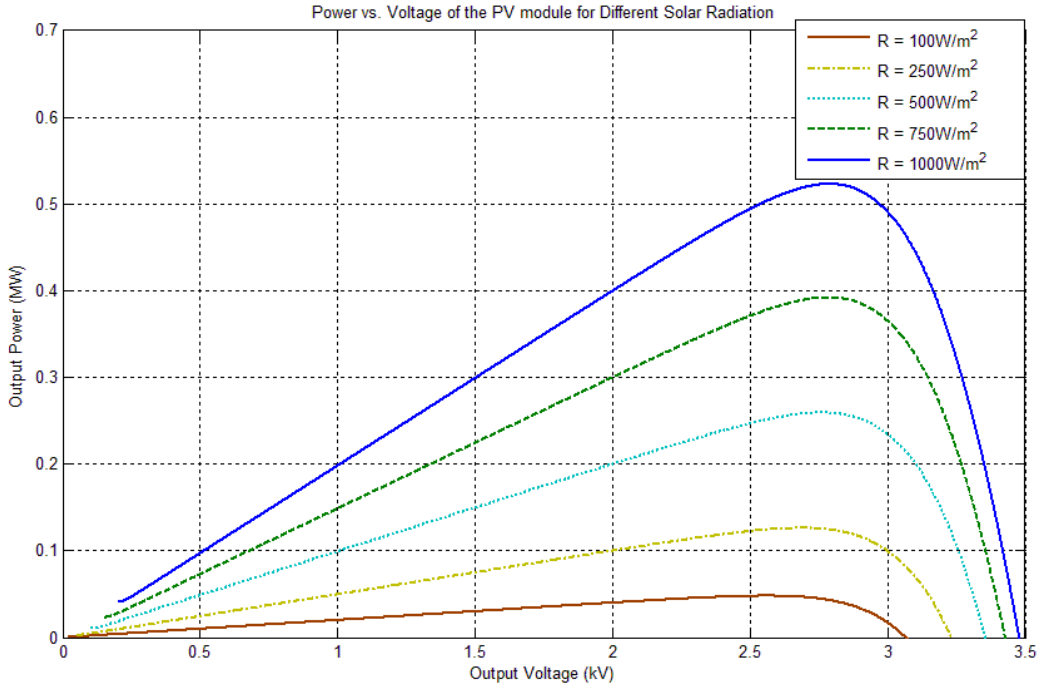

Fig. 3.12. Output power vs. voltage for different solar radiation of the PV arrays

3.5. Energy Storage Source Model

As discussed in previous sections, the droop control method is not used for the inverter control for DER units in the microgrid system. During the microgrid islanding process, the energy storage source (ESS) device is used to pick up the load immediately and enable the voltage and frequency control (V/F control) in the microgrid island operation mode. The most common energy storage devices include battery, super-capacitor, flywheel, superconducting magnetic energy storage (SMES), hydrogen, and compressed air. In this microgrid system, a DC battery was chosen to serve as the ESS unit.

A DC source was used for modeling a battery as energy storage source. An assumption has been made that the DC source can output as much power as required, so its limitation is not considered. A useful way to control the ESS in different modes was presented in the work of J. Y. Kim et al [29]. The ESS should be able to operate in PQ control mode when the microgrid is grid-connected, and it should also be able to operate in V/F mode when the microgrid is islanded. V/F mode means the ESS unit serves as a voltage source inverter, which sets the voltage and frequency values of the microgrid system.

The PQ mode control method is the same as used in the frequency converter for the wind energy source model. The method of V/F control mode is shown in Fig. 3.13. A feedback loop control for the output voltage RMS value was used. The overall control scheme of the ESS unit is shown in Fig. 3.14. When the microgrid is operating in grid-connected mode, the ESS unit operates in PQ control mode to output constant real and reactive power. When the microgrid transfers into the islanded mode, the ESS unit switches into V/F control mode to set up the system voltage and frequency values.

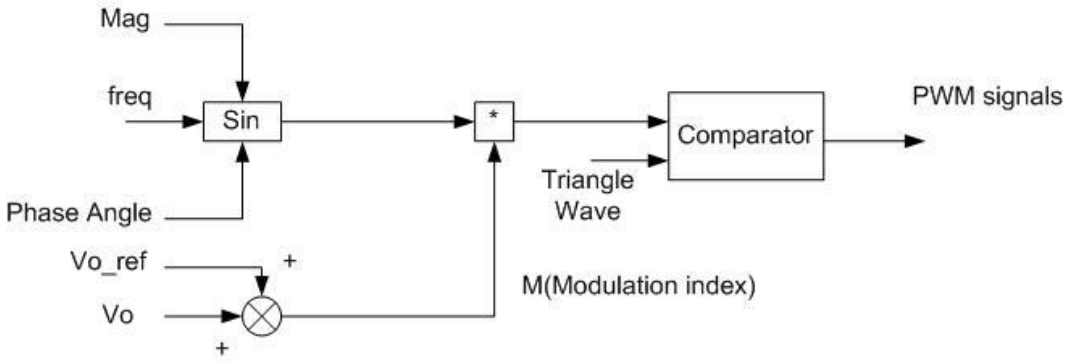

Fig. 3.13. The control method for V/F mode of the ESS unit

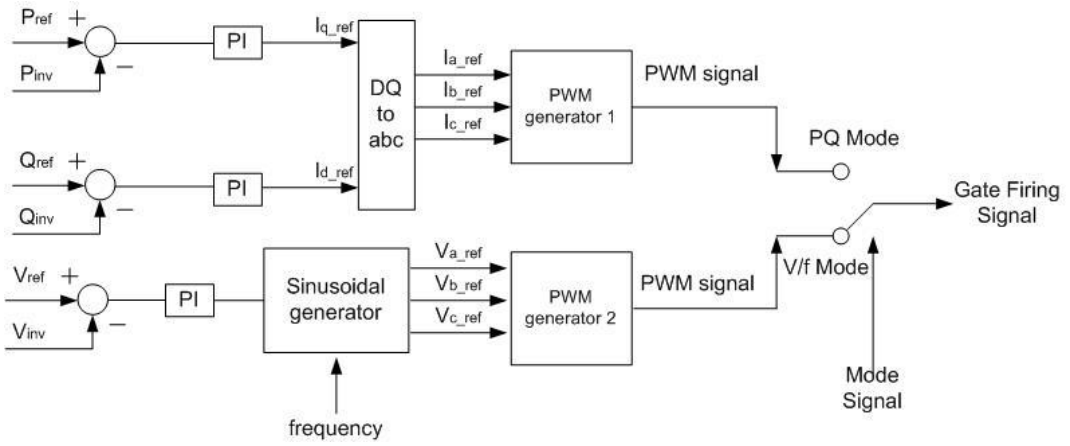

Fig. 3.14. The overall control scheme for the ESS unit

The ESS unit operating characteristics are shown in Fig. 3.15 for V/F control mode and Fig. 3.16 for PQ control mode. The x axis Pd is defined as the mismatch part between the total load in the microgrid and the output of other DER units. In V/F mode, the ESS picks up all of the mismatch part. In PQ control mode, the ESS output power is predetermined by a reference value.

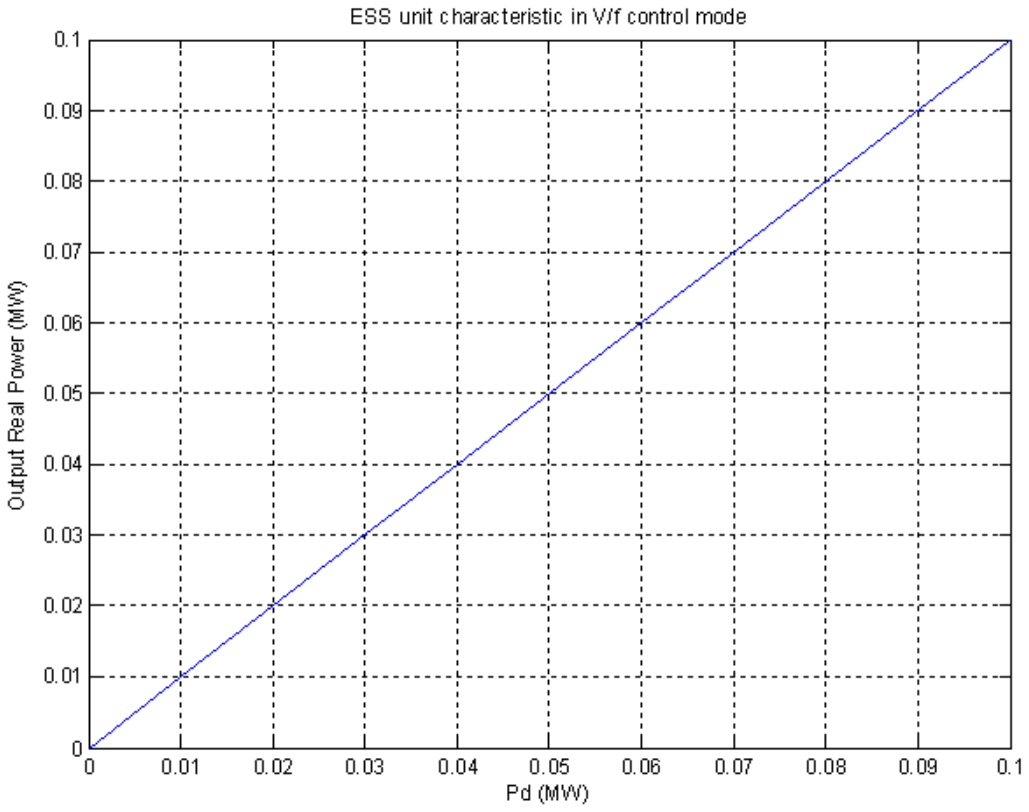

Fig. 3.15. ESS unit characteristics in V/F control mode

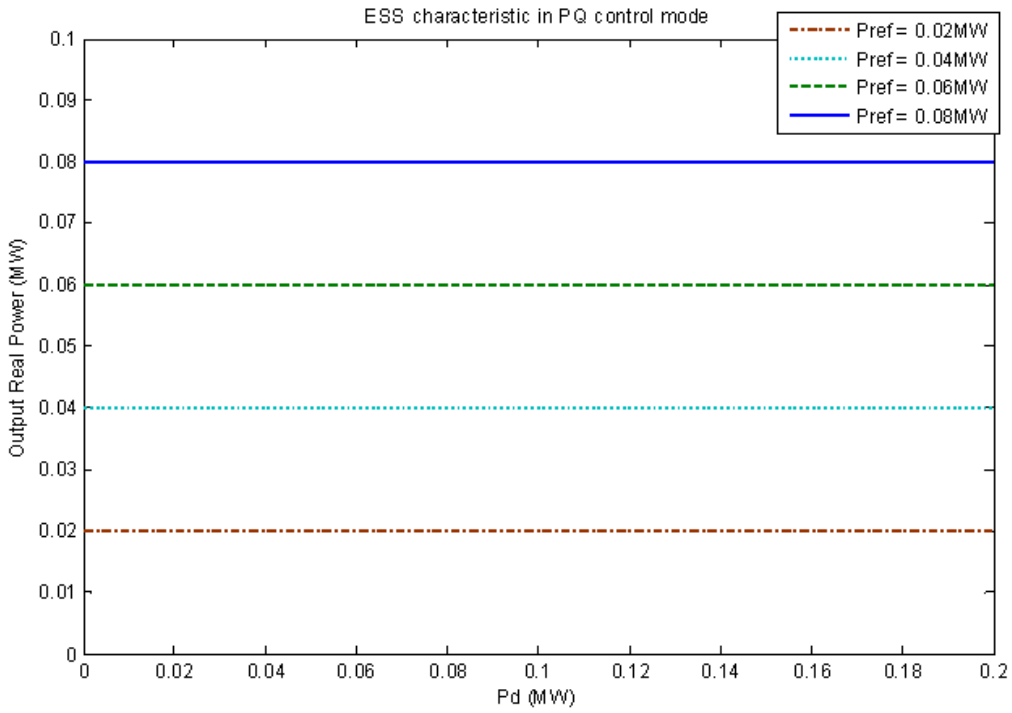

Fig. 3.16. ESS unit characteristics in PQ control mode

3.6. Protection Scheme and Component Models

Based on the system model, a protection scheme and the corresponding protective relay component models were developed. The relay components are able to monitor the currents and voltages in both phase and sequence domain. The protection components were coordinated so that they can protect the microgrid system from different faults, including single-line-to-ground (SLG) fault, line-to-line (LL) fault, etc.

The main structure of the proposed microgrid system is the same as the CERTS microgrid testbed. Thus a similar protection scheme as the CERTS Microgrid scheme was used [13].

The relay locations in the proposed microgrid are the same as the CERTS microgrid shown in Fig. 3.17. As shown in the figure, four main relays in the microgrid monitor the branch current and the node voltage levels. The protection schemes used in the microgrid are as follows [13]: 1) primary protection uses differential current and symmetric approach to protect a microgrid against all SLG and LL faults; 2) if the primary protection fails, the conventional over-current protection is the first back-up; 3) the second back-up are mainly under voltage monitoring. For the interconnection switch, the peak current limitation and the voltage quality are also monitored.

The protection scheme coordination is shown in Table 8. In this table, I_d is the differential current which defined as $I_d = RMS(\sum_{k=a,b,c,n} I_k)$. I_0 and I_- is the zero sequence and negative current flowing through the relays. I is the current RMS value. If any of those conditions in Table 8 happens, the protective relays will send corresponding tripping signals to the related breakers. Four relay component models in this work for Zone 2, Zone 3, Zone 4 and Zone 5.

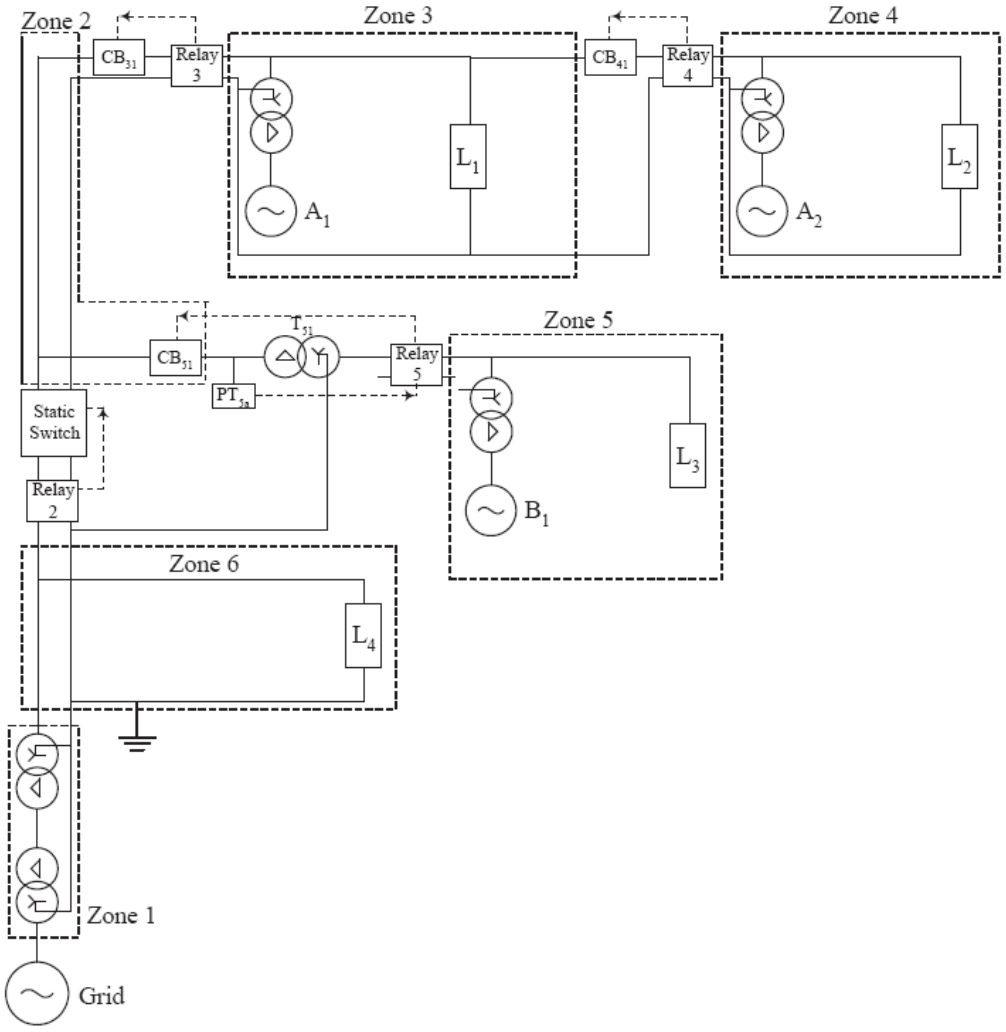

Fig. 3.17. Protective relays location in the CERTS microgrid [13]

Table 8 Protection scheme settings and coordination

Protection	Relay	Trip Conditions			Relay Type
		Up-stream SLG faults	Down-stream SLG faults	Line-to-Line faults	
Primary	2	I_d>50A Delay = 0ms	| I_0 |>15A Delay = 0ms	| I_-|>9A Delay = 0ms	a. Residual current b. Zero-sequence current c. Negative sequence current
	3	I_d>50A Delay = 167ms	| I_0 |>15A Delay = 167ms	| I_-|>15A Delay = 50ms	
	4	I_d>50A Delay = 50ms	| I_0 |>15A Delay = 50ms	| I_-|>9A Delay = 50ms	
	5	I_d>50A Delay = 50ms	|I0|>15A Delay = 50ms	| I_-|>15A Delay = 50ms	
1st Back-up	2	|I|>480A, ABB-Westinghouse CO-8			Time overcurrent
	3	|I|>225A, ABB-Westinghouse CO-8			
	4	|I|>125A, ABB-Westinghouse CO-8			
	5	|I|>125A, ABB-Westinghouse CO-8			
2nd Back-up	2	Peak Current |I|>750A	Voltage power quality levels		a. Instantaneous over current b. Under voltage c. Over/under frequency
	3		50% under voltage delay 30 cycles		Under voltage
	4		50% under voltage delay 30 cycles		
	5		50% under voltage delay 30 cycles		

The interconnection switch is controlled by protective relay 2, which is more complicated than other relays. Basically, the interconnection switch should be able to

disconnect the microgrid from the utility grid under the following conditions [30]: 1) poor voltage quality from the utility, like unbalances due to nearby asymmetrical loads; 2) frequency of the utility falls below a threshold, indicating lack of generation on the utility side; 3) voltage dips that last longer than the local sensitive loads can tolerate; 4) faults in the system that keep a sustained high current injection from the grid; 5) any current that is detected flowing from the microgrid to the utility system for a certain period of time. These functions are incorporated into the protective relays for the interconnection switch.

The settings of the relays were coordinated with ideal AC sources instead of the DER units. Therefore the protection scheme needs future proper enhancement to obtain correct performances.

4. SIMULATION CASE STUDIES

4.1. Introduction

4.1.1. Objective of Simulation Case Studies

The objective of the simulation case studies was to verify that the proposed microgrid simulation model can operate in different modes with high DER penetration, and to analyze its performance and operational scenarios.

4.1.2. Assumptions and Limitations of Simulation Case Studies

In PSCAD simulation software, there are always start-up transients due to the initializing and computing requirement in the software. For example, the starting-up process of a synchronous generator in PSCAD is a complicated process [24]. The start-up sequence includes three steps. First, at time t = 0s, the machine is modeled as a simple fixed three-phase voltage source at its terminals, while its voltage magnitude and phase is as entered by the user. Second, after a certain time period, the machine switches from an ideal voltage source to a machine with constant speed. The mechanical dynamics are not in place during this period and the rotor will be spinning at a constant speed corresponding to the base angular frequency specified by the user. Finally, after another time period, the machine switches from a constant speed machine to a variable-speed machine. In this work, the machine switches to step two at t = 0.25s and switches to step three at t = 0.5s. At the point in time when the machines are running free and the excitation and governor systems are stable a snapshot can be taken, which allows the

user to use the condition at this time point to be the initial conditions for the following simulation.

The DC and AC sources in PSCAD also include initial ramp up time to reach steady state. The start-up transient occurs during the initializing of the software, which is usually not taken into consideration when doing analysis.

The largest switching frequency of the power electronics devices in the system is 10 kHz. In order to obtain reasonable results for the power electronics related simulation, the time step was set to be 10 us for all of the cases, which is considered to be valid and reasonable in the case studies. The channel plot time step was set to be 50 us, which is small enough for most variables.

The basic one-line diagram of the microgrid system for the simulation case studies is shown in Fig. 4.1. The monitored variables included voltage, current, power and other variables of the DER units and the measurement points 2, 3, 4, 5, 6 in Fig. 4.1. The instantaneous values of voltage and current were measured directly. The calculated voltage RMS value and three-phase real and reactive power in were smoothed through a real pole function to simulate a transducer delay and to reduce output ripple by the meter component in PSCAD. The time constant of the real pole function was left to its default value of 0.02s in each measurement.

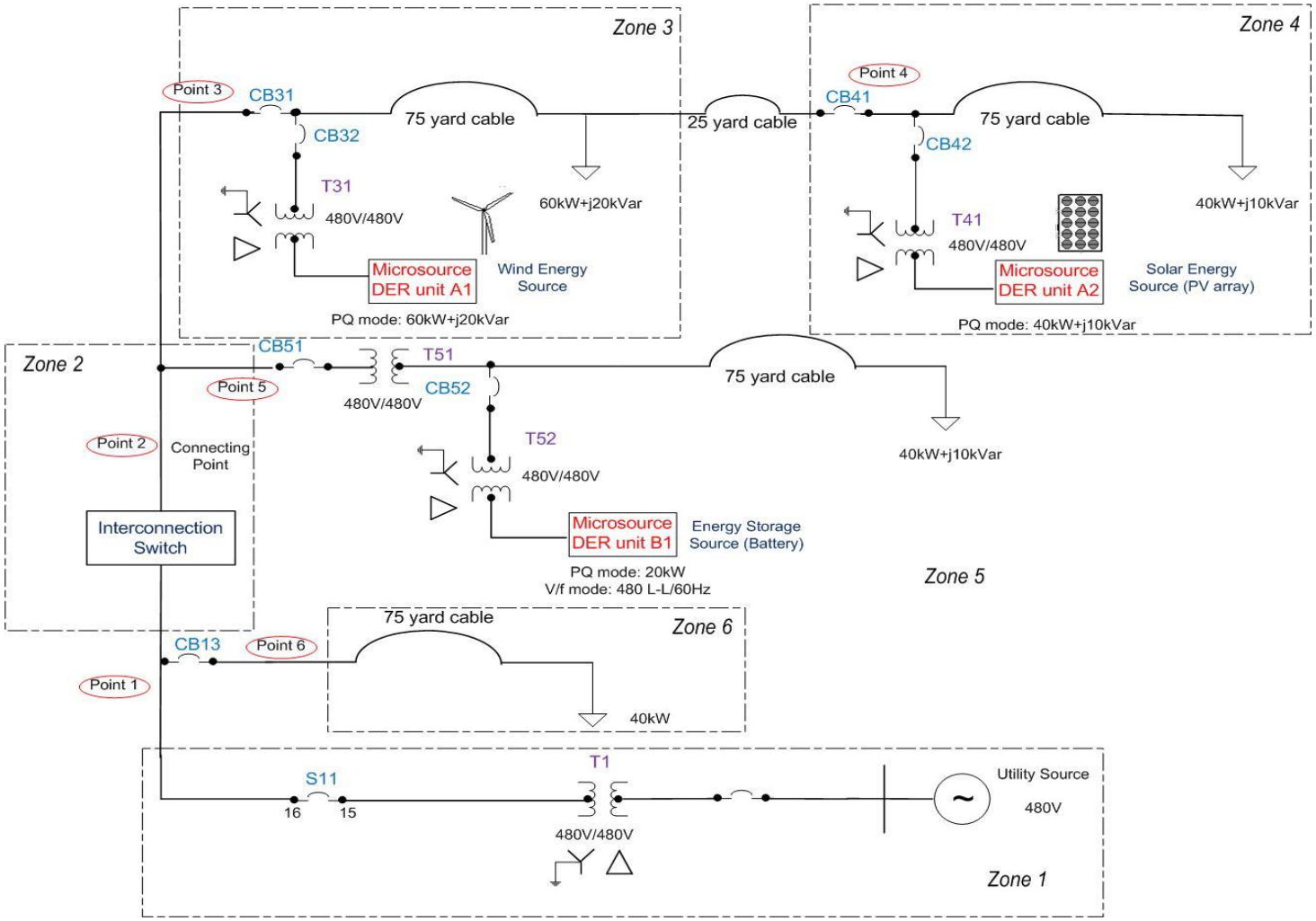

Fig. 4.1. One-line diagram of the microgrid system for case studies

4.1.3. Overview of the Simulation Case Studies

A 480V AC source served as the utility grid connection. The system included three DER units: one ESS unit, one wind energy source and one solar energy source. A group of simulation case studies were conducted. Many variables in the system could be monitored. As shown in Fig. 4.1, the point 2, 3, 4, 5 and 6 are actually the locations for protective relays in each zone. The line-to-line voltage RMS values were measured. For each DER units, the output real power and reactive power were monitored. Some other important parameters were also measured.

Since the PQ control mode was used for the wind and the solar energy sources, the input parameters of the wind turbine and PV array did not influence the results as long as the reference power value was smaller than the DER unit output limitation. The wind and solar energy source would reach their steady state operating points according to the output power references. In the simulation case studies, the default input wind speed for the wind source model was set to be 12m/s, the default solar radiation of the PV arrays was set to be $600W/m^2$, and the cell temperature was set to be 50℃.

4.2. Simulation Case Studies

4.2.1. Case Study 1: The Steady State

Case Study 1 presented the microgrid system reaching a steady state after the start-up transient. In this case, all of the three DER units operated in PQ control mode. The power output references and the load levels were set as shown in Table 9. The initial output power references of these three units were set to be 20kW, 60kW+j20kVar and

40kW+j10kVar respectively. The load banks in three zones were 60kW+j20kVar, 40kW+j10kVar and 40kW+j10kVar. Thus in Case 1, the total output power of the DER units was 120kW+j30kVar, and the total load level in the microgrid was 140kW+20kVar. The mismatch part was expected to be supplied by the utility grid.

Table 9 The DER units power references and load levels in each zone in Case 1

	Load Level		DER unit output reference values	
	Real load level (kW)	Reactive load level (kVar)	DER unit output real power (kW)	DER unit output reactive power (kVar)
Zone 3	60	20	60	20
Zone 4	40	10	40	10
Zone 5	40	10	20	0
Zone 6	40	0	NA	NA

The simulation running stopped after t = 10s. The output real power values of the DER units are shown in Fig. 4.2. The corresponding reactive power values are shown in Fig. 4.3. The values of real and reactive power injected by the utility grid are shown in Fig. 4.4. Those figures show that after the start-up transient, the output power values of the DER units reached steady state values. The real power values for DER units were around 60kW, 40kW and 20kW. Take t =10s as example, at this time point, the DER units output are shown in Table 10, which were very close to the reference values in Table 9. The grid injected real and reactive power also reached steady state. The grid

injected reactive power was larger than the load requirement value because of the leakage reactance of the transformers.

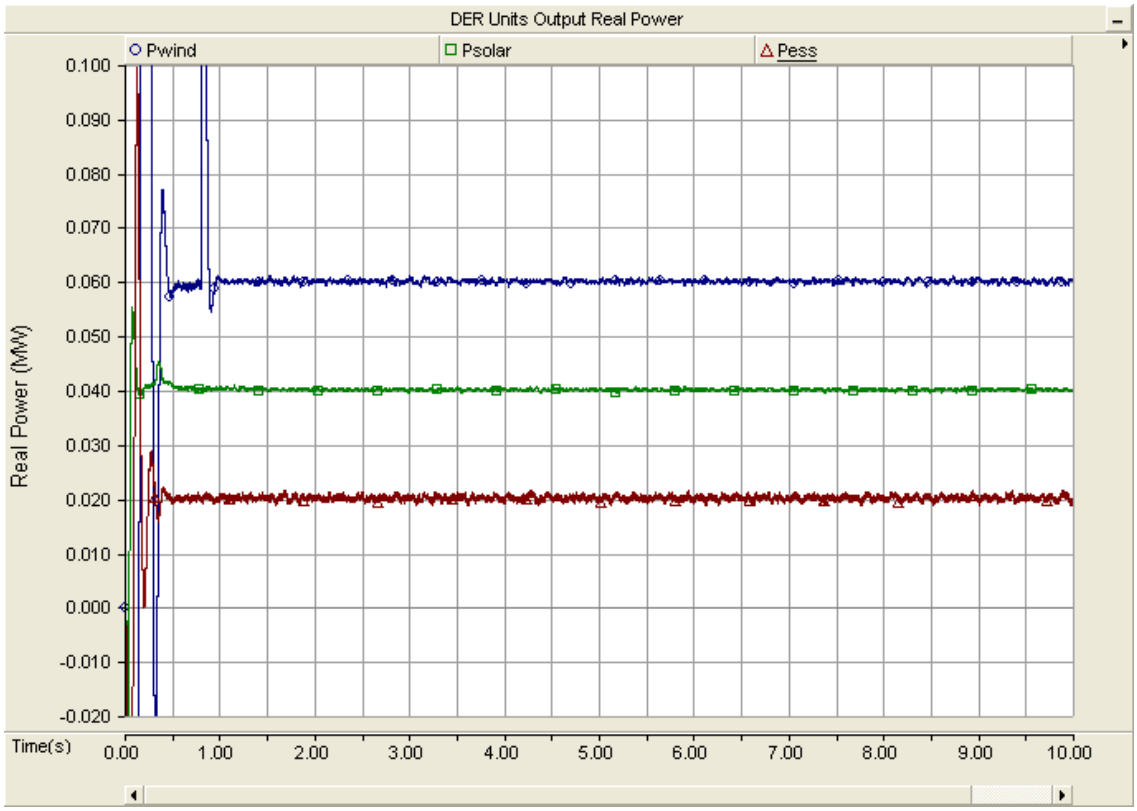

Fig. 4.2. Real power output values of DER units in Case 1

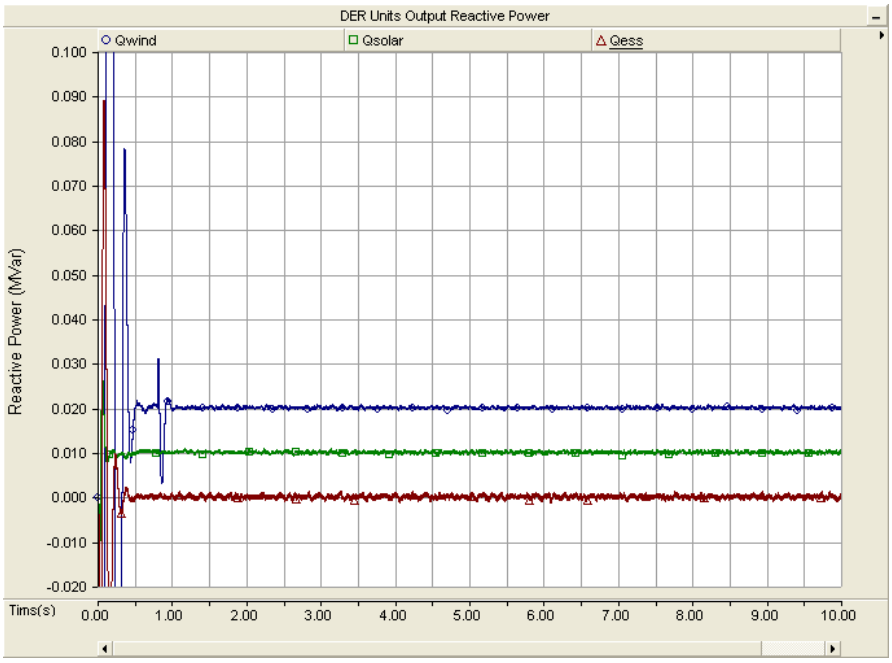

Fig. 4.3. Reactive power output values of DER units in Case 1

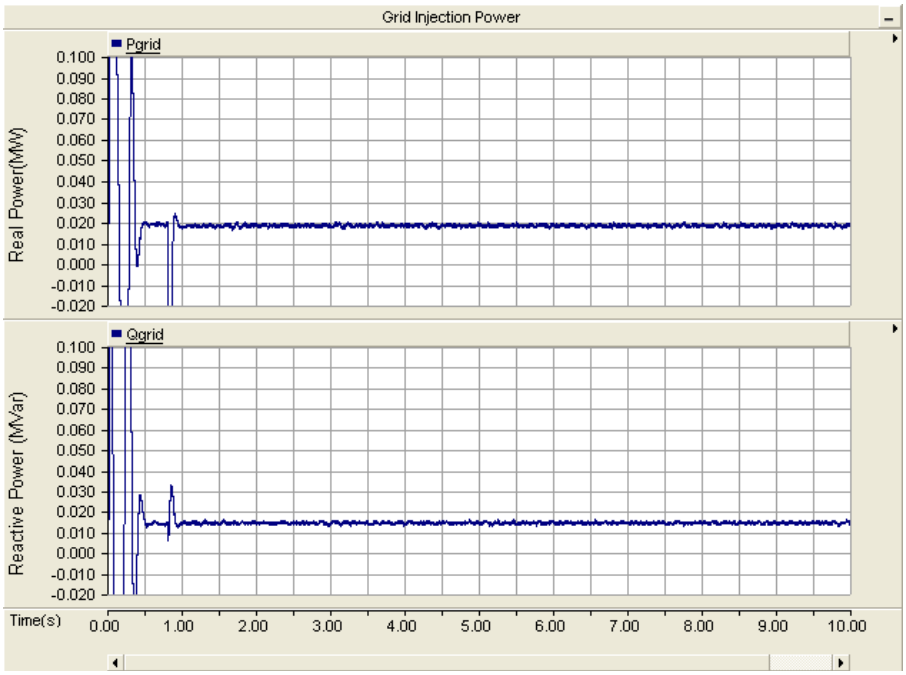

Fig. 4.4. Power injected from the utility grid in Case 1

The line-to-line voltage RMS values of the measurement points at t =10s are shown in Table 11. All of these RMS values were close to the rated value at 480V.

The wind turbine output power and mechanical torque are shown in Fig. 4.5. The output power and rotor speed of the synchronous machine which connected with the wind turbine are shown in Fig. 4.6. These two figures show that the wind turbine and synchronous generator reached steady state after the start-up process. The output power of the wind turbine was about 67kW, slightly larger than the output power of the synchronous generator about 60kW, which is due to the efficiency of the synchronous generator around 89%.

The output voltage, current and power of the PV arrays are shown in Fig. 4.7, which indicates that the PV arrays also reached steady state.

Table 10 The output power of DER units in Case 1 at t = 10s

	Real power output (kW)	Reactive power output (kVar)
Microsouce A1 (Wind Energy Source)	60.0	19.9
Microsouce A2 (Solar Energy Source)	40.1	10.3
Microsouce B1 (Energy Storage Source)	20.2	0
Grid Injecting	18.8	14.3

Table 11 The line-to-line voltage RMS values at the measurement points in Case 1 at t = 10s

	Point 2	Point 3	Point 4	Point 5	Point 6
Line-to-line Voltage RMS (V)	479.8	479.7	477.7	479.5	475.4

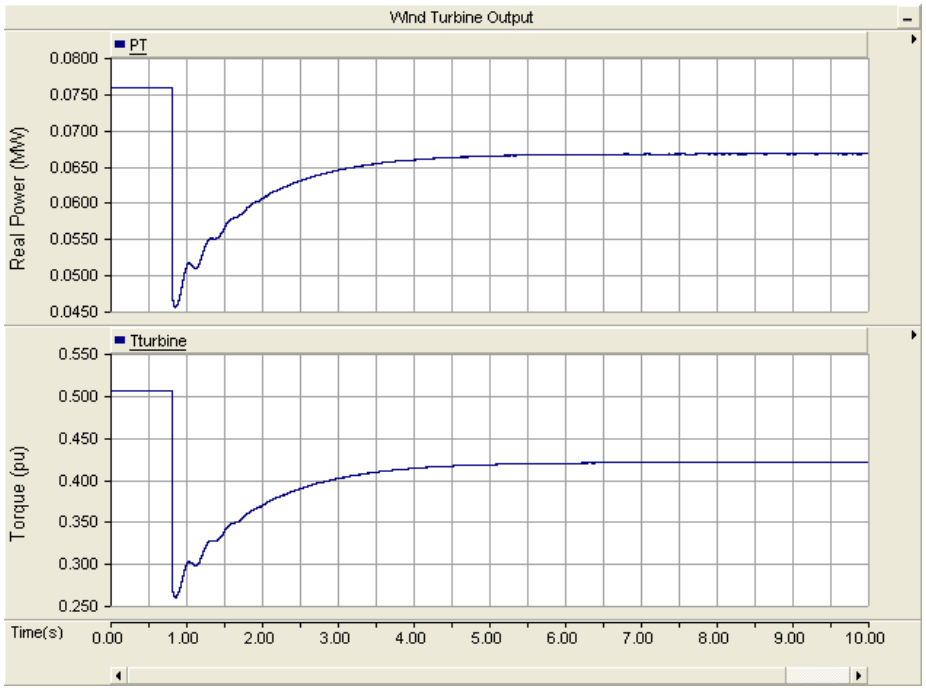

Fig. 4.5. Wind turbine output power and mechanical torque in Case 1

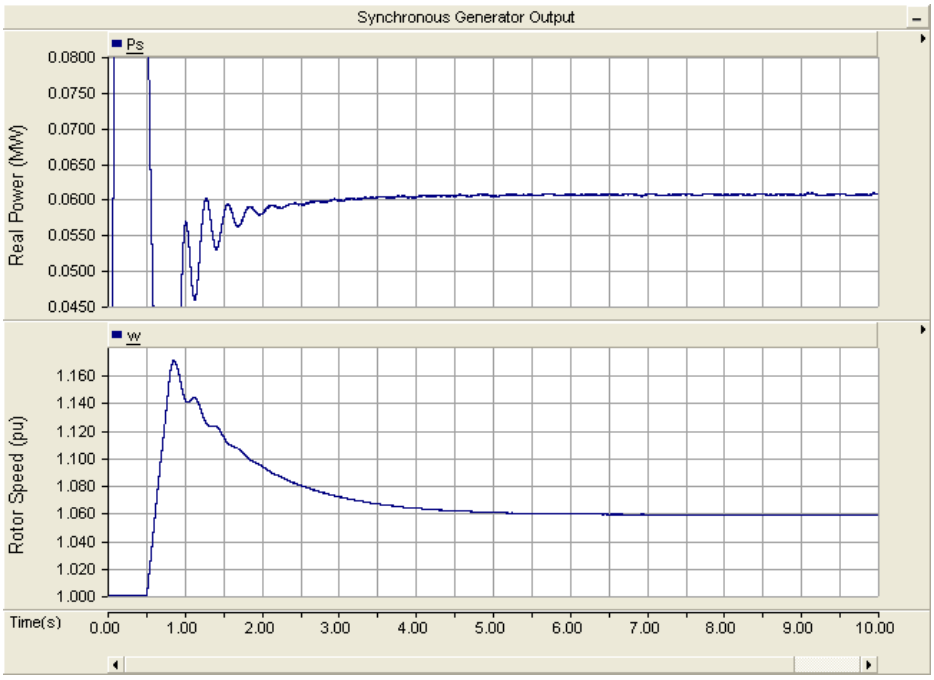

Fig. 4.6. The synchronous generator output power and mechanical speed in Case 1

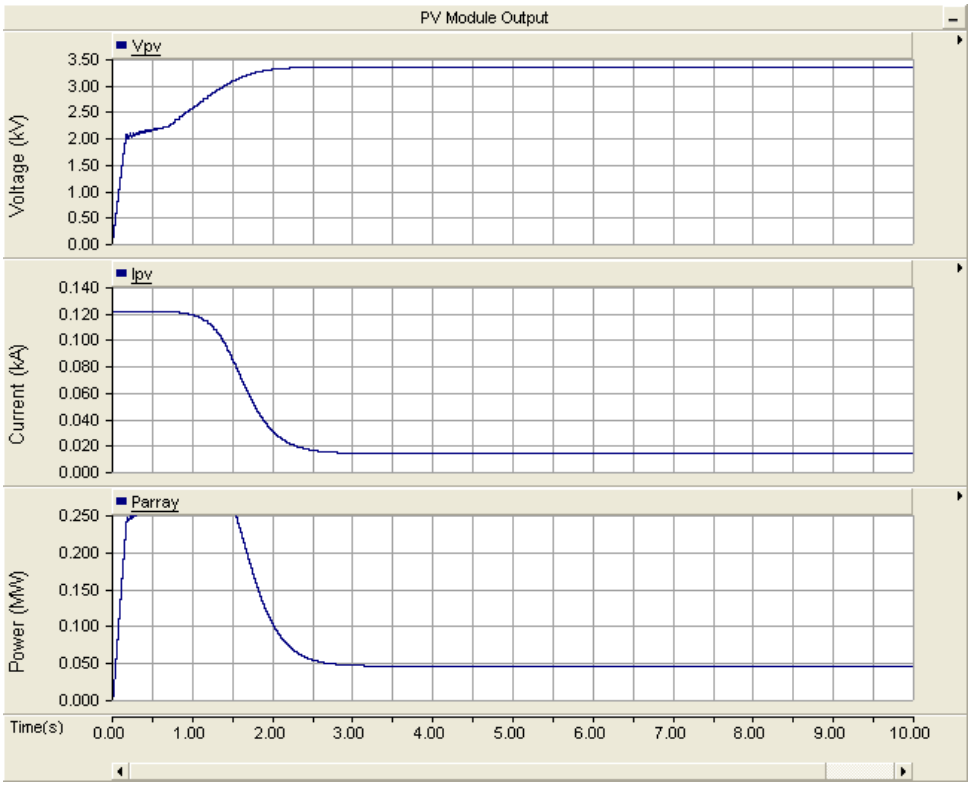

Fig. 4.7. The PV arrays responses in Case 1

The simulation results in Case 1 show that the PQ control method applied to the DER units effectively controlled the output real power and reactive power. The wind energy source and the solar energy source worked as expected.

As discussed in previous part, the start-up transient is required for initializing computation in the software, which is usually not taken into consideration when doing analysis. The most important part in this case was the final steady state it reached. After the system entered steady state in Case 1, a snapshot was taken at t = 10s, which saved the system steady state condition for the following case studies to use. All of the

following case studies were applied after the system reached steady state, which means the following case studies started with the conditions in Case 1 at time = 10s.

4.2.2. Case Study 2: The Impact of Changes in DER Units

Case Study 2 presents the impact of changes in DER units in microgrid. The load level and the power references of DER units were the same as in Case 1. The output power references of three DER units were set to be 20kW, 60kW+j20kVar and 40kW+j10kVar respectively. The load banks in three zones were 60kW+j20kVar, 40kW+j10kVar and 40kW+j10kVar.

a) Case 2a: The impact when the input wind speed changed for the wind source model in the microgrid

In Case 2a, the input wind speed for the wind turbine changed from 12m/s to 13m/s at t = 0.5s. The output real power values of the DER units at are shown in Fig. 4.8, and the corresponding reactive power values are shown in Fig. 4.9. The wind turbine outputs are shown in Fig. 4.10. The synchronous generator responses are shown in Fig. 4.11. Those figures show that when the wind speed suddenly changed to a new value, the output power of the inverter part of the wind energy source model did not change but still held as reference values. Inside the wind energy source model, the wind turbine output power increased immediately. This extra energy led the synchronous generator rotor speed to increase. Since the synchronous generator mechanical speed was the same as the rotor speed of the wind turbine, the output power of wind turbine then decreased. After a certain time period, the wind turbine output power and its mechanical speed reached a new steady state operating point.

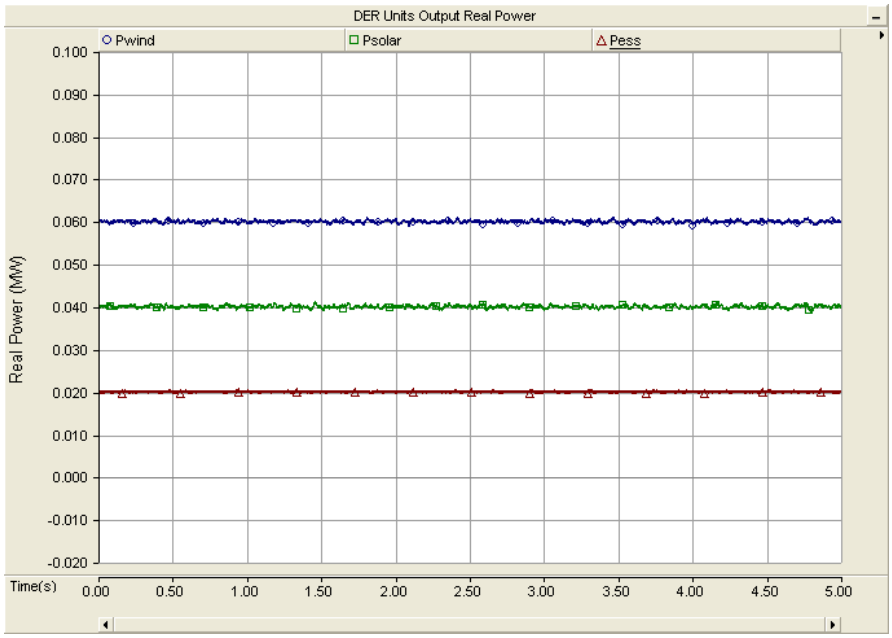

Fig. 4.8. Real power output values of DER units in Case 2a

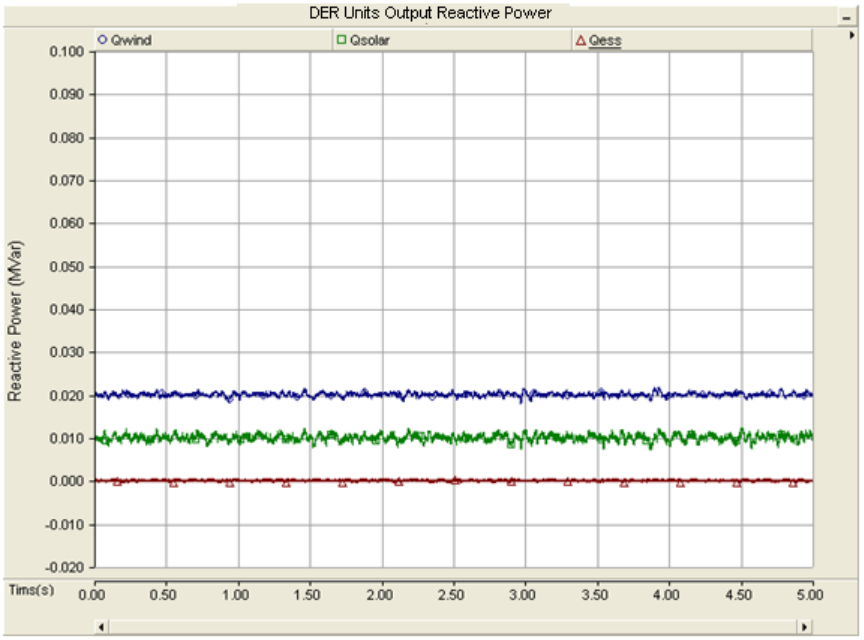

Fig. 4.9. Reactive power output values of DER units in Case 2a

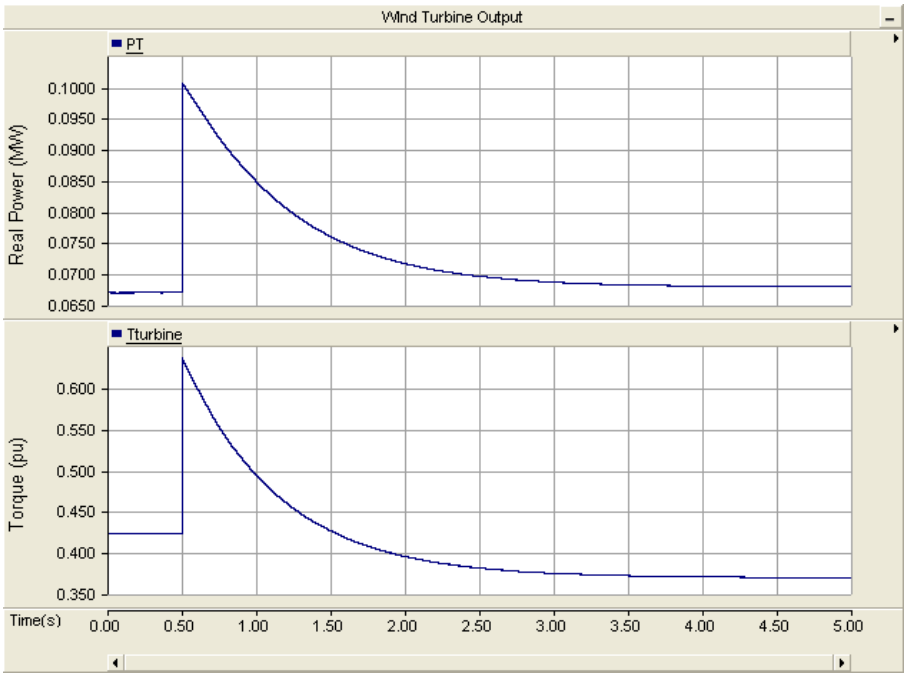

Fig. 4.10. Wind turbine output power and mechanical torque in Case 2a

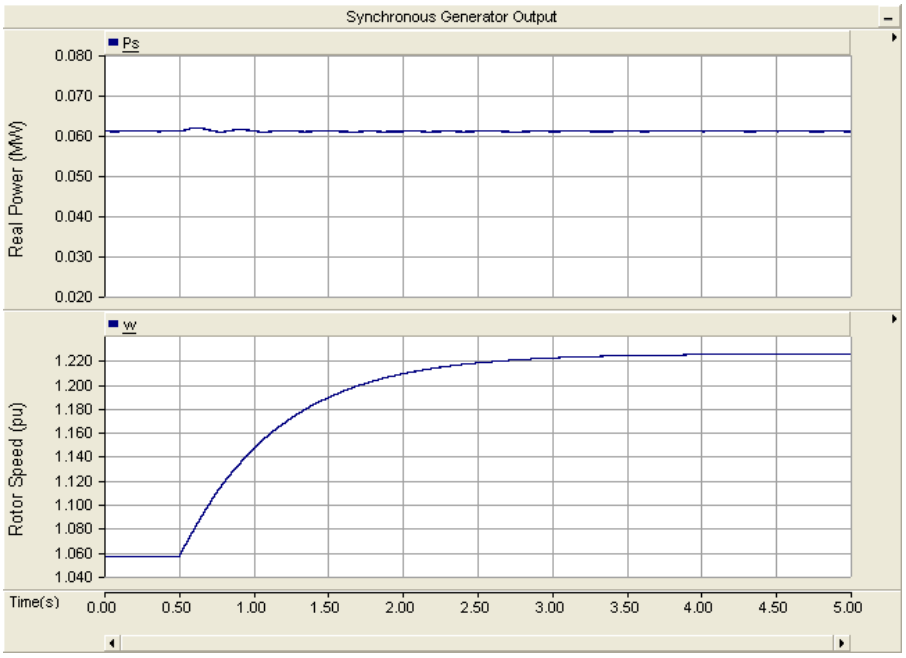

Fig. 4.11. The synchronous generator responses in Case 2a

b) Case 2b: The impact when the solar radiation changes for the solar energy source in the microgrid

In Case 2b, the solar radiation changed from 600 W/m^2 to 750 W/m^2 at t = 0.5s. The output real power values of the DER units are shown in Fig. 4.12. The corresponding reactive power values are shown in Fig. 4.13. The PV arrays responses are shown in Fig. 4.14. Those figures show that when the solar radiation suddenly changed to a new value, the output power of the inverter part of the solar energy source model did not change but still held as reference values. Inside the solar energy source model, the PV modules output power increased immediately. This extra energy led the output DC voltage of the PV arrays to increase and the capacitor absorbed the extra energy. The PV output current decreased as the voltage increased. After a certain time period, the PV output current and its voltage reached a new steady state operating point.

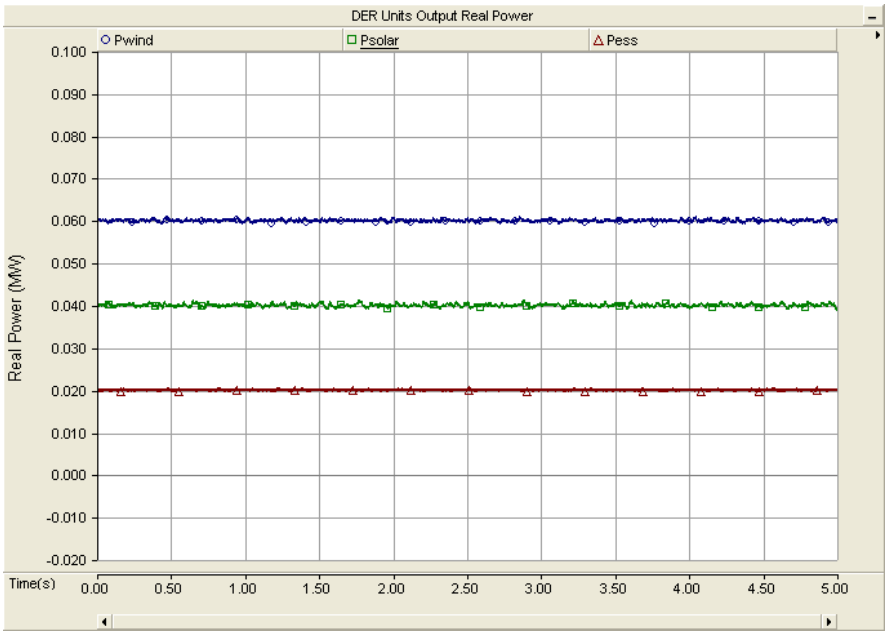

Fig. 4.12. Real power output values of DER units in Case 2b

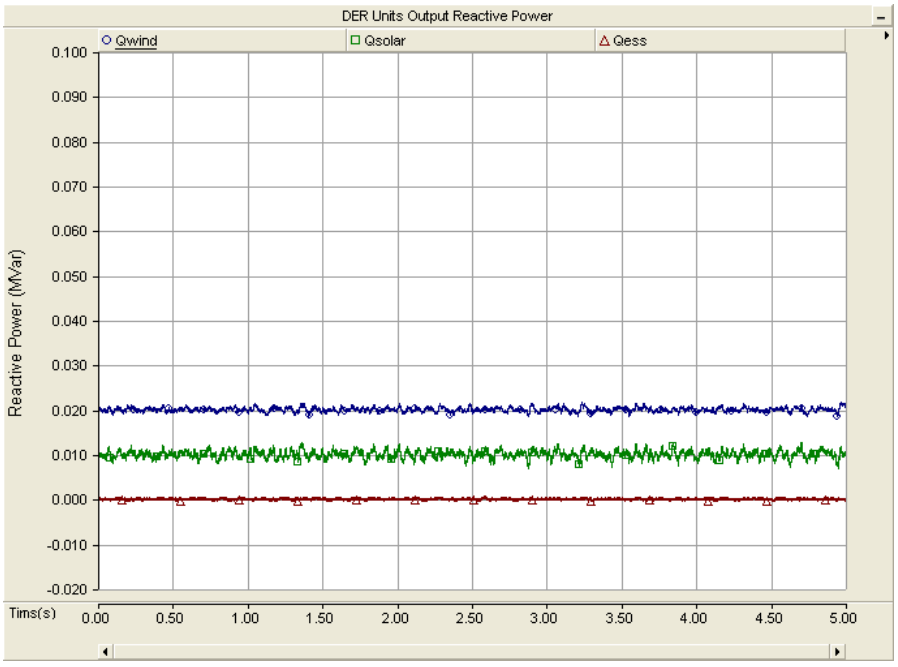

Fig. 4.13. Reactive power output values of DER units in Case 2b

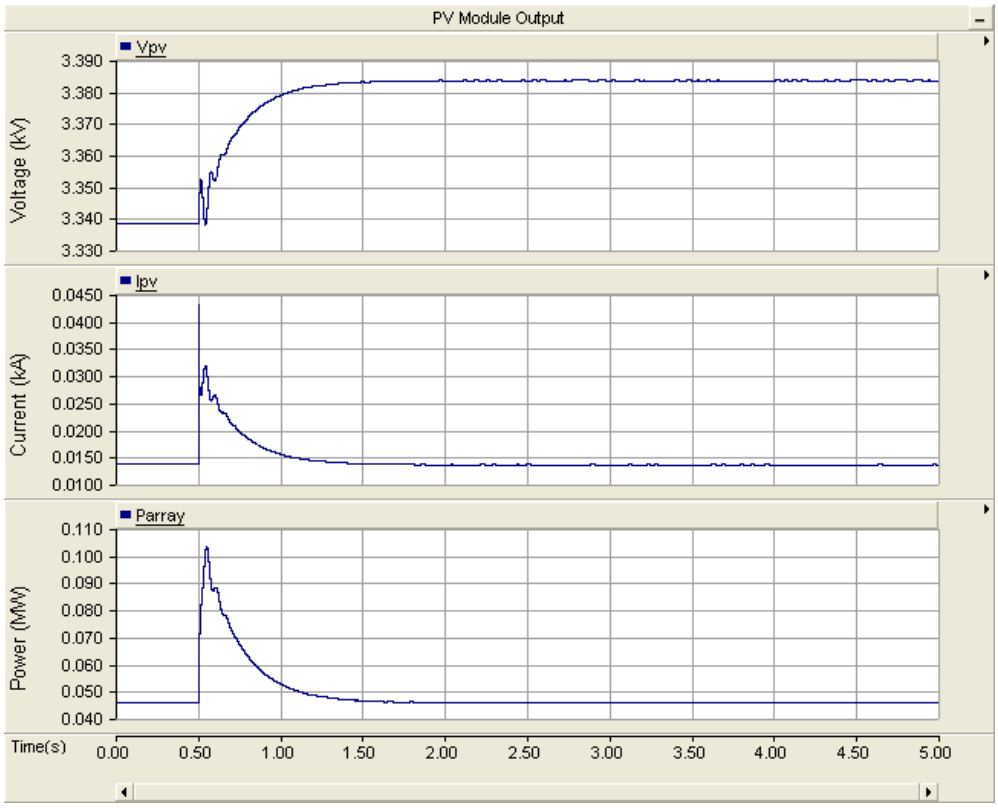

Fig. 4.14. The PV arrays responses in Case 2b

Case 2 showed that in the grid-connected mode, when a limited change occurred inside of the DER units, the DER units reached a new steady state after transients. This case showed the PQ control method for the DER units were effective. However, in this case the power references for the DER units did not change as the wind speed and solar radiation changed. Therefore the efficiency is not optimized, which needs to be improved in the future work such as incorporating the maximum power point tracking function into the wind energy source model and the solar energy source model.

4.2.3. Case Study 3: The Impact of Load Changes in Grid-connected Mode

Case Study 3 presents the impact when the load changes in the microgrid. Case Study 2 presented the impact of changes in DER units in microgrid. Two sub-cases were conducted. In Case 3, the initial load level and power references of the DER units were the same as in Case 1. The output power references of three DER units were 20kW, 60kW+j20kVar, and 40kW+j10kVar, respectively. The load banks in three zones were 60kW+j20kVar, 40kW+j10kVar and 40kW+j10kVar.

a) Case 3a: The impact of resistive load changes

Case 3a presents the impact when the resistive load changes in the micogrid. The resistive load in Zone 5 changed from 40kW to 60kW at t = 1s. The simulation stopped at t = 2.5s.

The output real power values for the DER units are shown in Fig. 4.15, and the reactive power values for the DER units are shown in Fig. 4.16. The values of real and reactive power values injected by the grid are shown in Fig. 4.17. It shows that in the grid-connected mode when these three DER units were in PQ control mode, the resistive load changed in the microgrid at t = 1s was picked up by the grid. The DER units output real and reactive power did not change during this process.

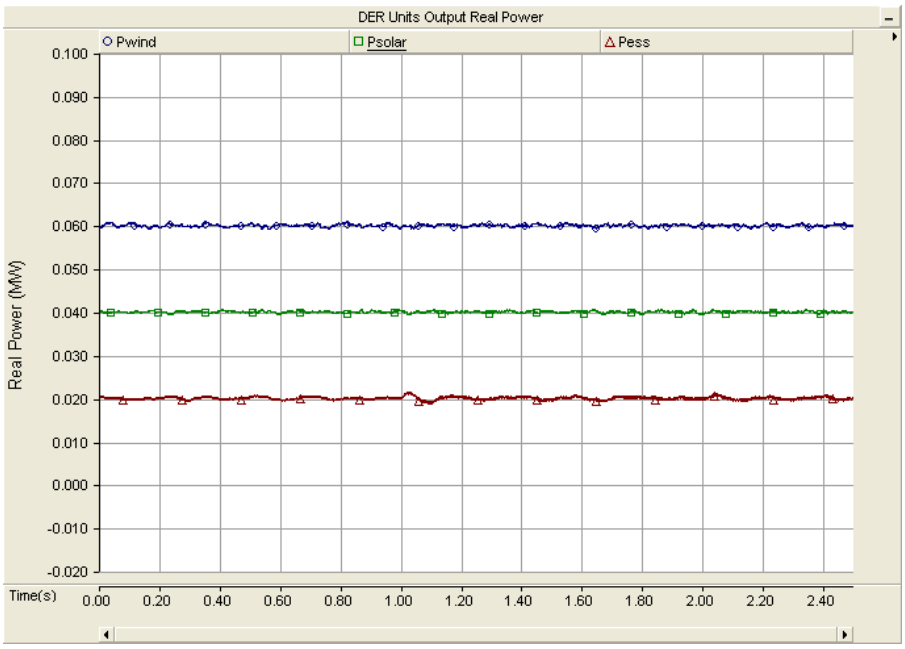

Fig. 4.15. Real power output values of DER units in Case 3a

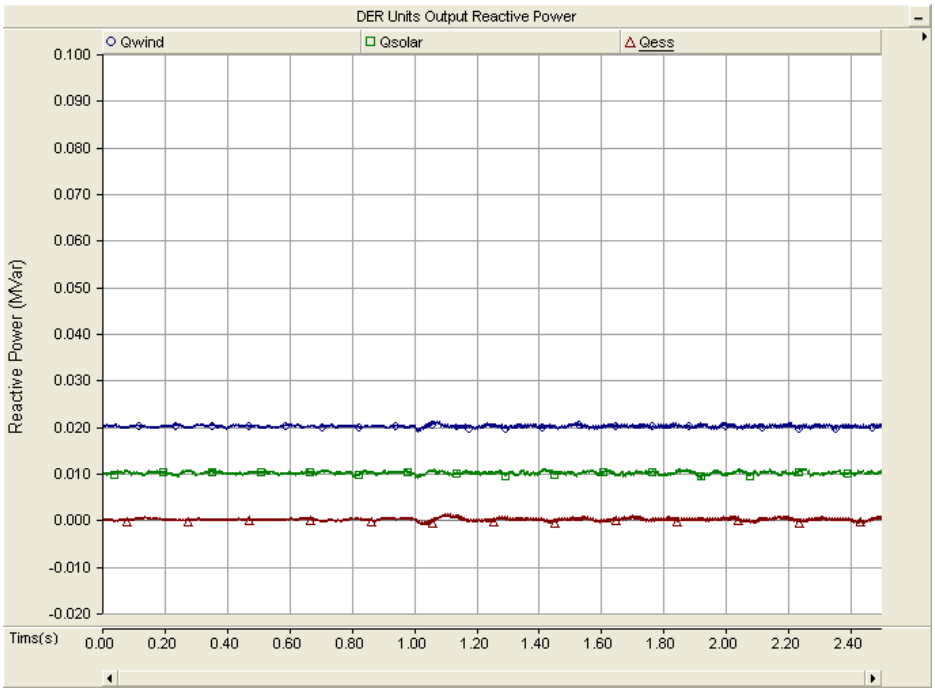

Fig. 4.16. Reactive power output values of DER units in Case 3a

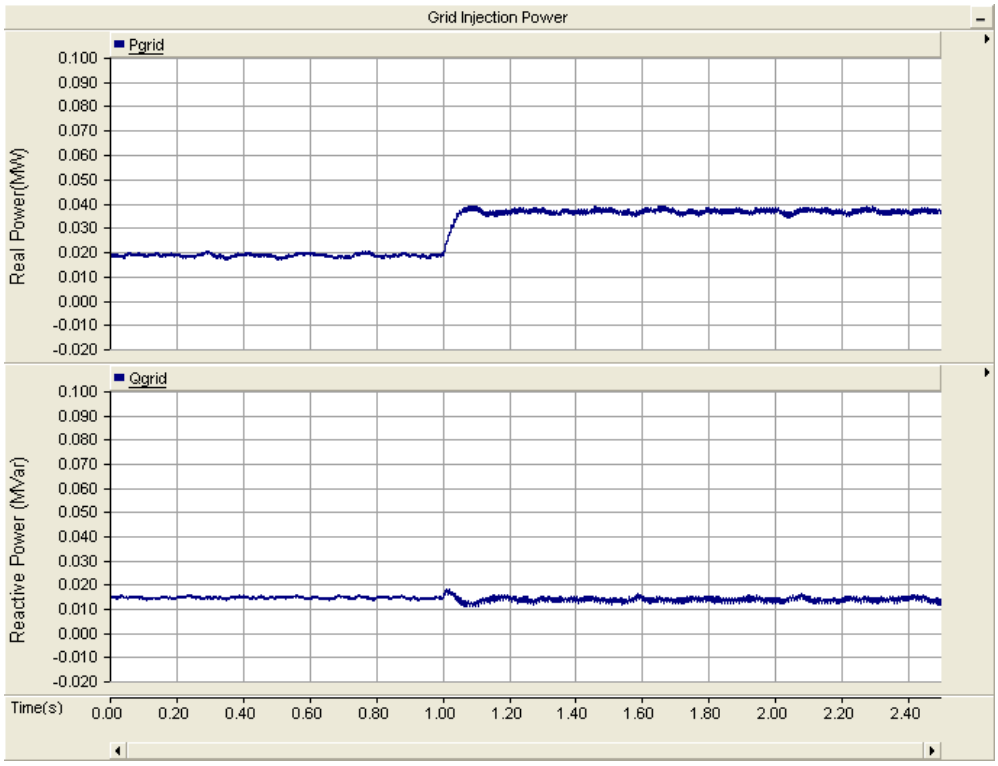

Fig. 4.17. Power injected from the utility grid in Case 3a

(b). Case 3b: The impact of inductive load changes

Case 3b presents the impact when the inductive load changes in the microgrid. The inductive load in Zone 5 changed from 0 to 10 at t = 1s. The simulation stopped at t = 2.5s.

The output real power values for the DER units are shown in Fig. 4.18, and the reactive power values for the DER units are shown in Fig. 4.19. The values of real and reactive power values injected by the grid are shown in Fig. 4.20. It shows that in the grid-connected mode when these three DER units were in PQ control mode, the

inductive load changed in the microgrid at t = 1s led the grid injected reactive power decrease. The DER units output real power and reactive did not change during this process.

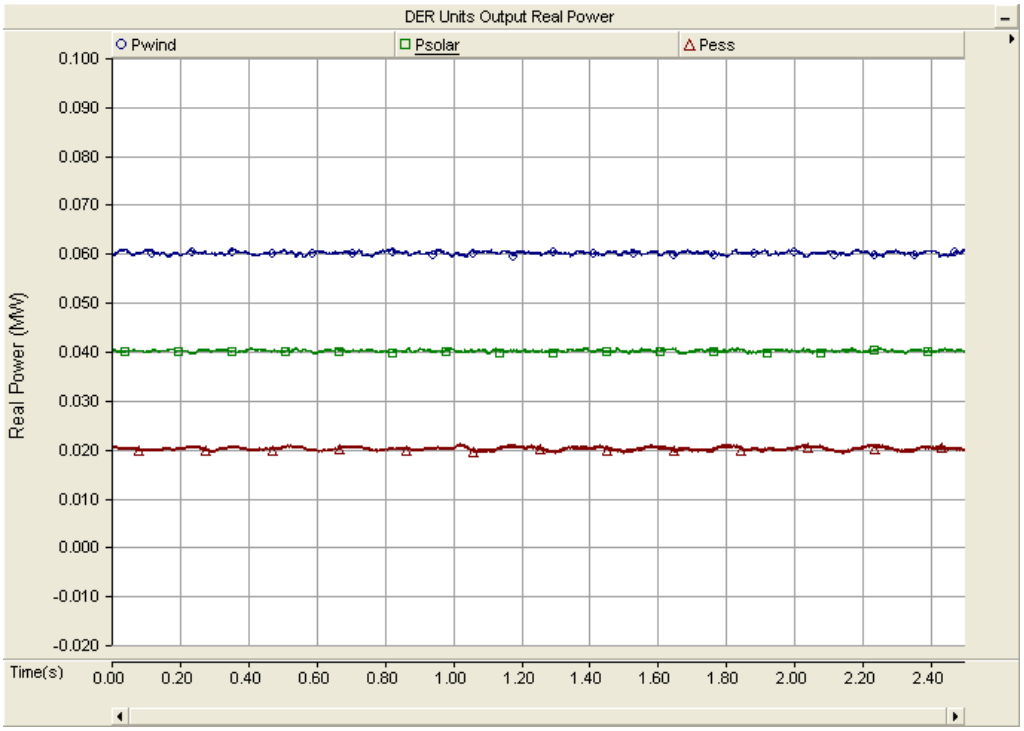

Fig. 4.18. Real power output values of DER units in Case 3b

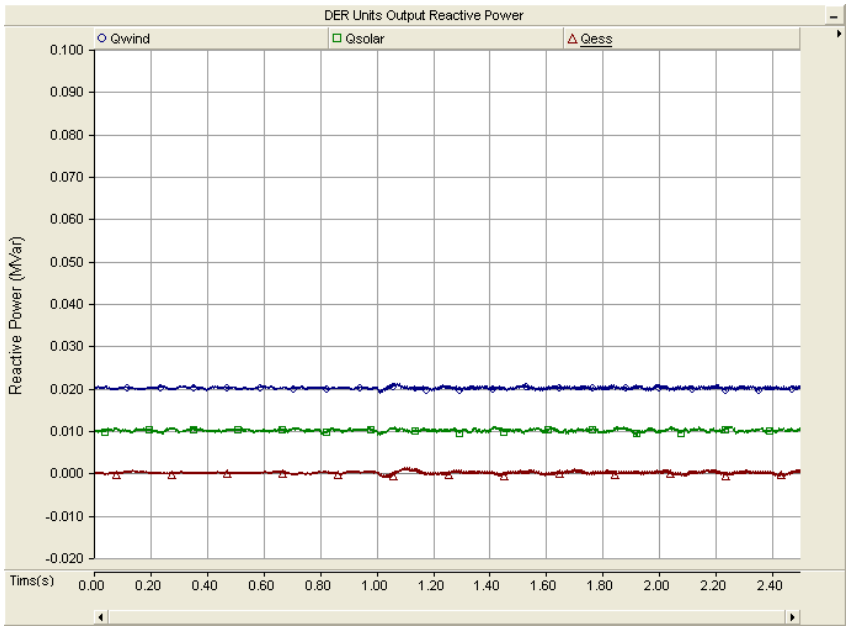

Fig. 4.19. Reactive power output values of DER units in Case 3b

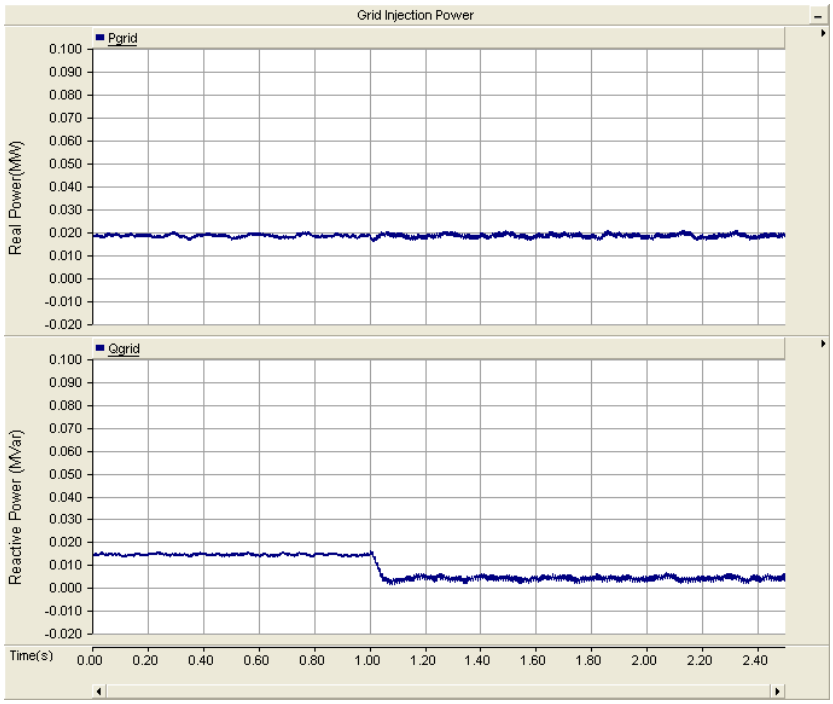

Fig. 4.20. Power injected from the utility grid in Case 3b

The simulation results in Case 3 show that when the resistive or inductive load changes in the microgrid where all the DER units operate in PQ control mode, the changing of the real power or reactive power demand did not influence the DER units. The changed part of the load was picked up by the utility grid.

4.2.4. Case Study 4: Pre-planned Islanding

The objective of this study was to investigate transient behavior of the micro-grid due to a pre-planned islanding process. Prior to the islanding, the system initial settings were the same as in Case 1. The initial output powers of these three units were set to be 20kW, 60kW+j20kVar, and 40kW+j10kVar, respectively. The load banks in three zones were 60kW+j20kVar, 40kW+j10kVar and 40kW+j10kVar. The load part supplied by the grid was 20kW+j10kVar. At = 1s, the interconnection switch was opened and the microgrid transferred from the grid-connected mode into the islanded mode.

The simulation stopped at t = 2.5s. The output real power values for the DER units are shown in Fig. 4.21, and the reactive power values for the DER units are shown in Fig. 4.22. The values of real and reactive power values injected by the grid are shown in Fig. 4.23. Those figures show that after the islanding process, the mismatch part of the load in the microgrid was totally picked up by the ESS unit after transients. Take t =2.5s as example, at this moment, the DER units output are shown in Table 12. The wind and solar energy sources output power values were still around the reference values.

The line-to-line voltage RMS value at point 5 is shown in Fig. 4.24. The instantaneous output voltage of the ESS unit when the microgrid transferred into

islanded mode at t = 1s is shown in Fig. 4.25. These two figures show that after a transient the system voltage level could be maintained to the expected value. The line-to-line voltage RMS values of the measurement points at t = 2.5s are shown in Table 13. All of these values were close to 480V rating.

Wind turbine output power and mechanical torque are shown in Fig. 4.26. The synchronous generator output power and mechanical speed are shown in Fig. 4.27. The PV arrays responses are shown in Fig. 4.28. These figures indicate that the wind and solar energy sources experienced very small transients during the islanding process, and after that they reached a new steady with the reference power outputs.

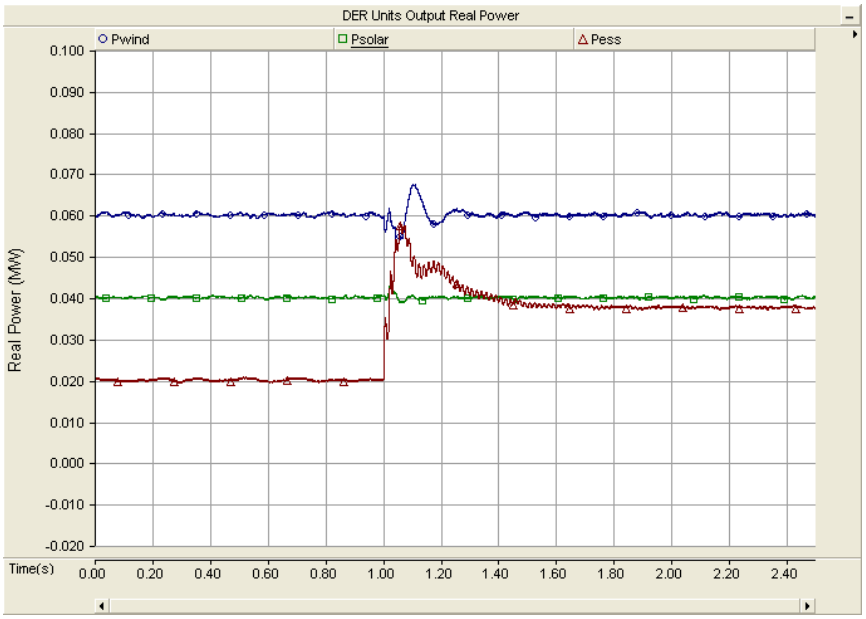

Fig. 4.21. Real power output values of DER units in Case 4

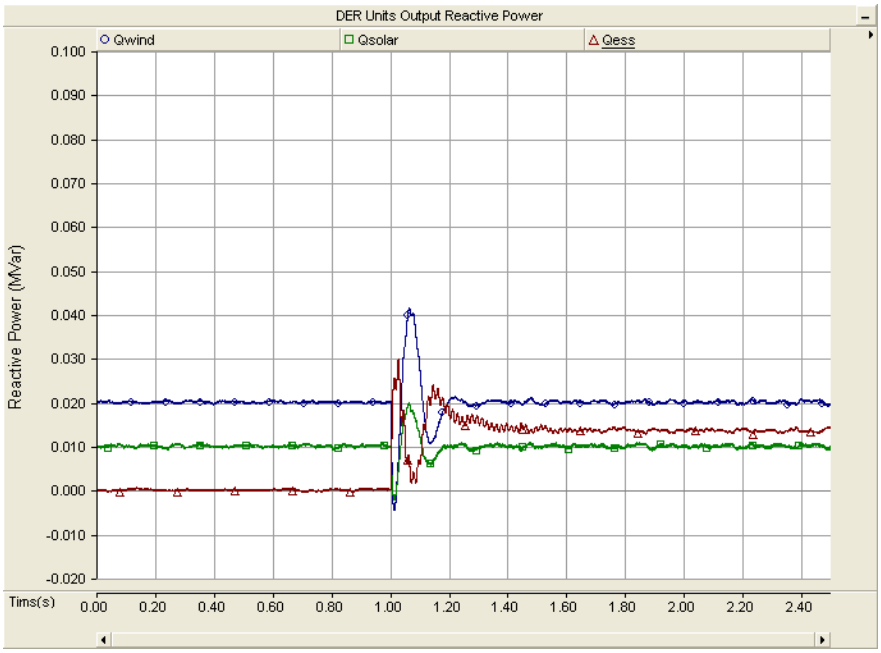

Fig. 4.22. Reactive power output values of DER units in Case 4

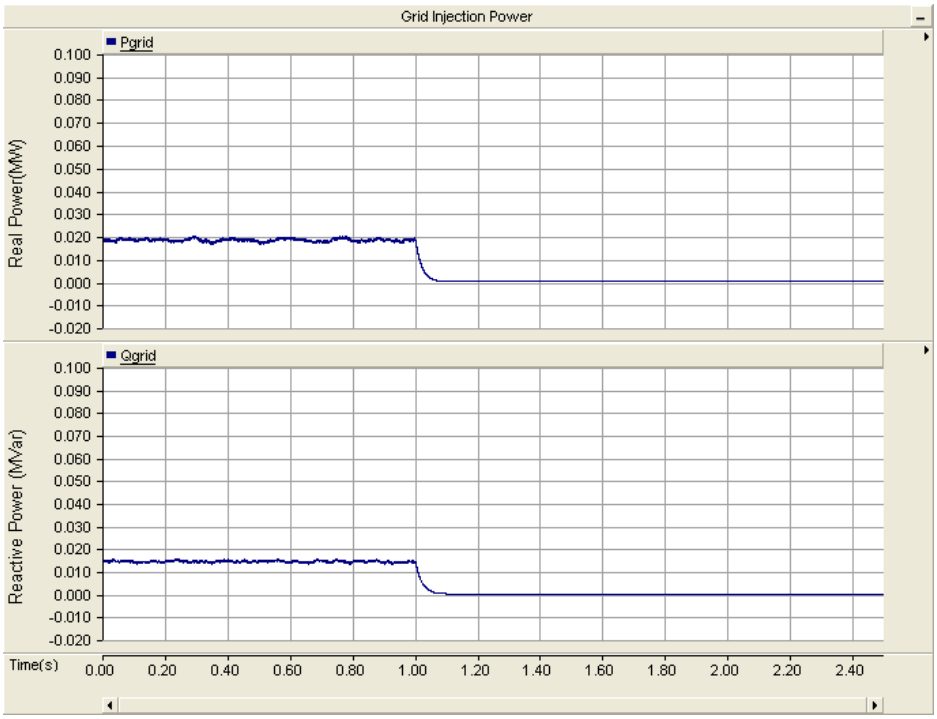

Fig. 4.23. Power injected from the utility grid in Case 4

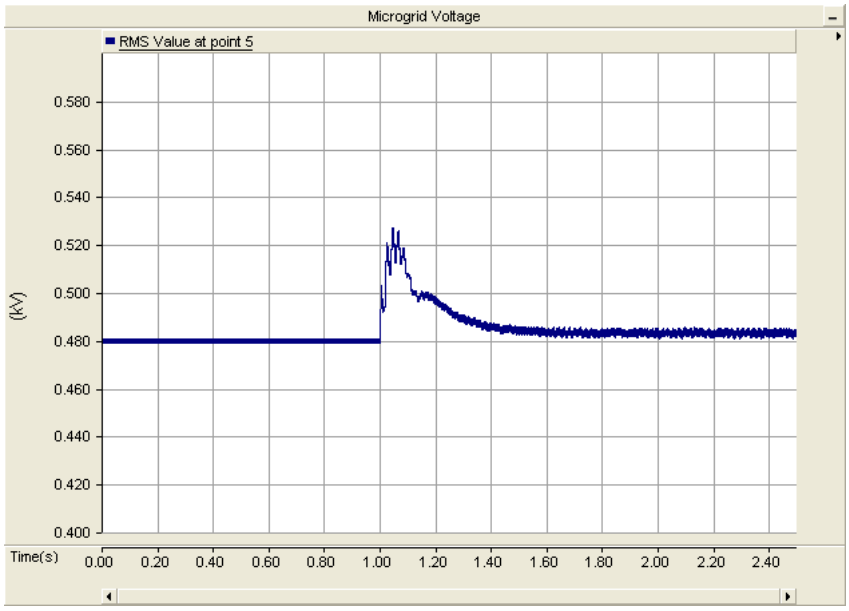

Fig. 4.24. The line-to-line voltage RMS value at point 5 in Case 4

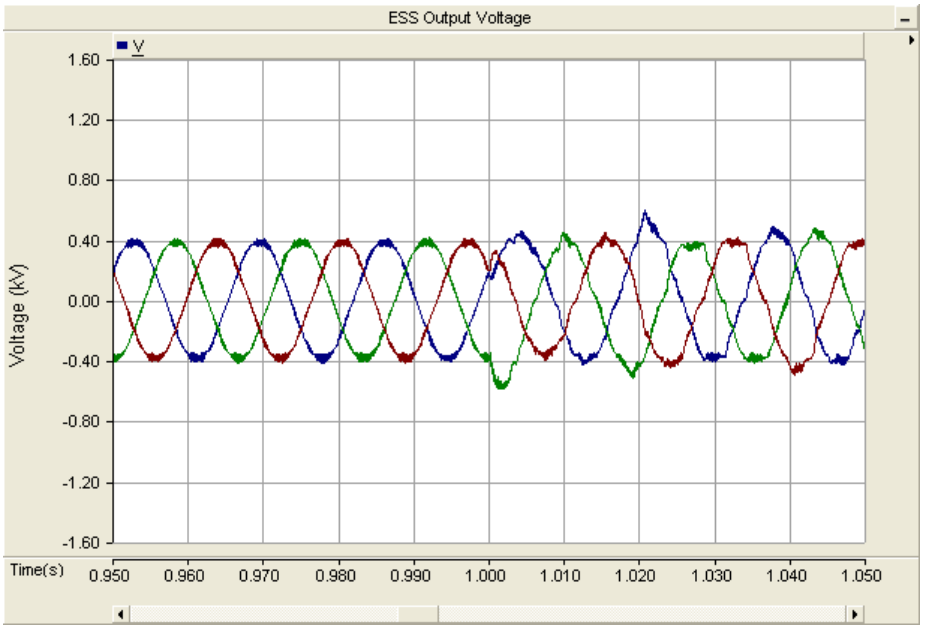

Fig. 4.25. The instantaneous output voltage of the ESS unit when the microgrid transfers into islanded mode at t = 1s in Case 4

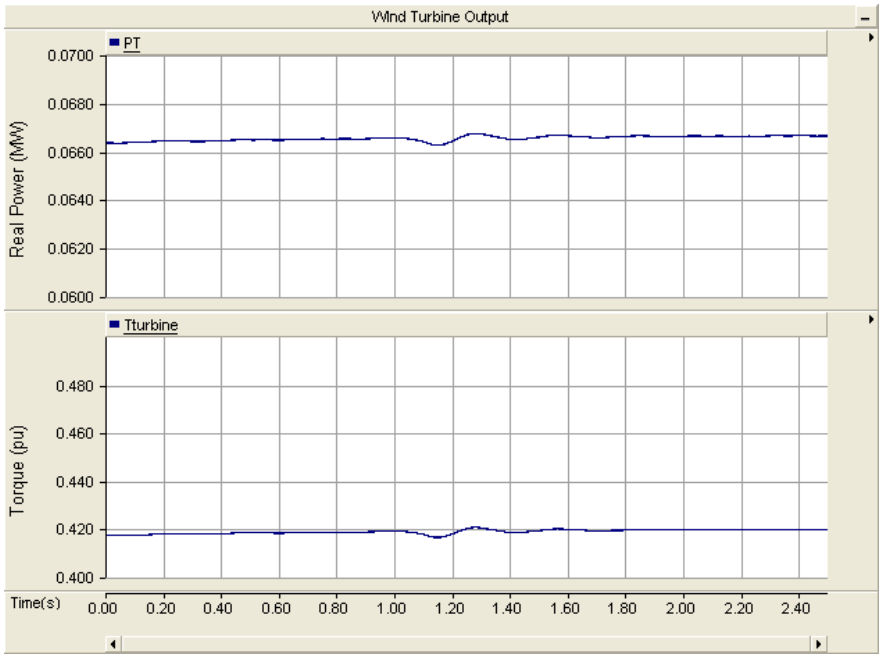

Fig. 4.26. Wind turbine output power and mechanical torque in Case 4

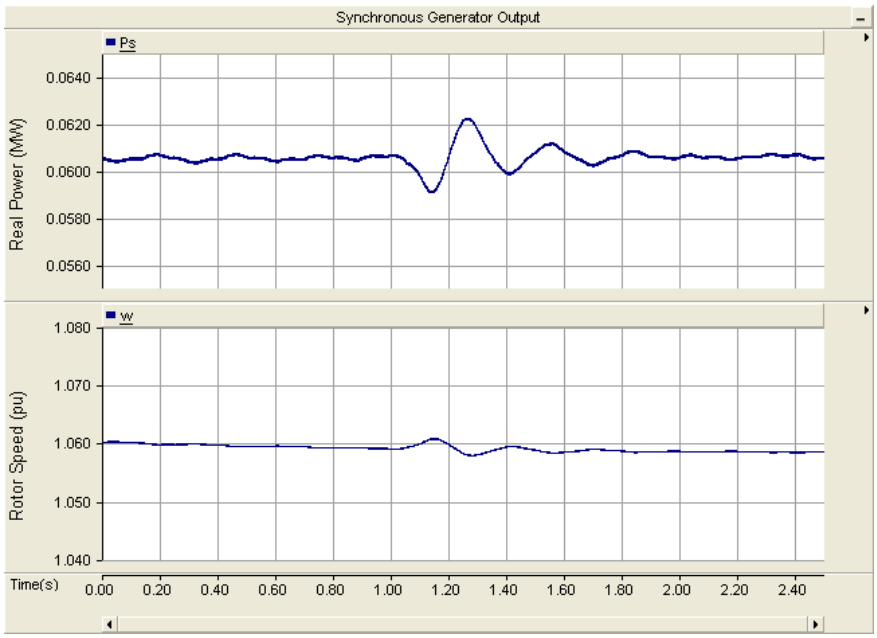

Fig. 4.27. The synchronous generator output power and speed in Case 4

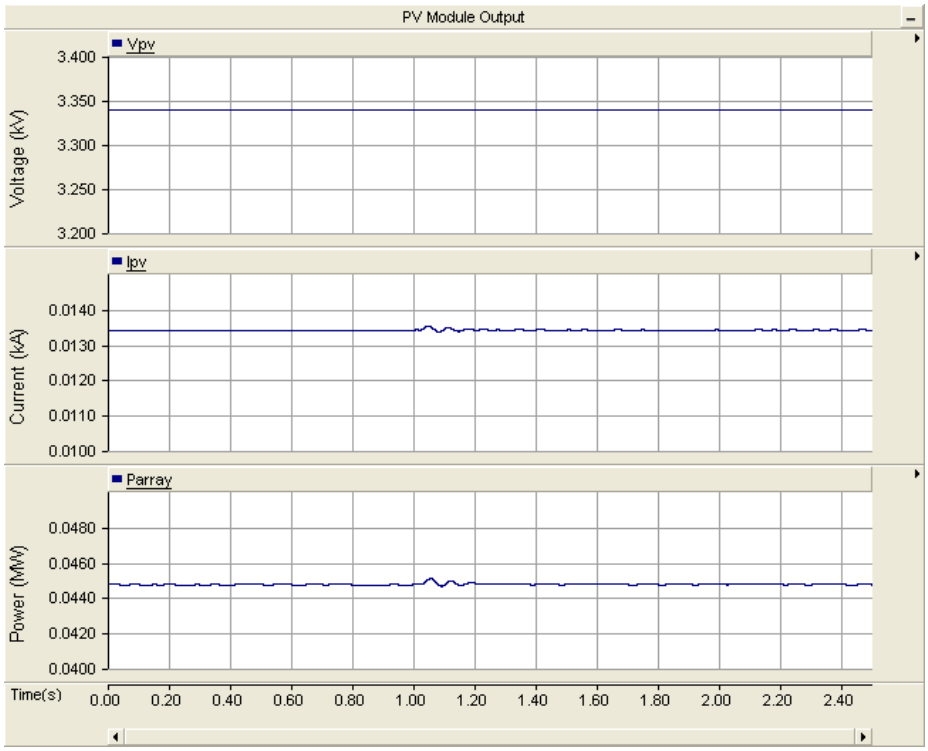

Fig. 4.28. The PV arrays responses in Case 4

Table 12 The output power of DER units in Case 4 at t = 2.5s

	Real power output (kW)	Reactive power output (kVar)
Microsource A1 (Wind Energy Source)	59.4	19.6
Microsource A2 (Solar Energy Source)	40.1	9.9
Microsource B1 (Energy Storage Source)	37.3	14.0
Grid Injecting	0	0

Table 13 The line-to-line voltage RMS values at the measurement points in Case 4 at t = 2.5s

	Point 2	Point 3	Point 4	Point 5	Point 6
Line-to-line Voltage RMS (V)	479.7	479.6	476.8	481.4	475.3

The simulation results in Case 4 show that when a pre-planned islanding happened, the microgrid could successfully transfer from grid-connected mode into islanded mode after a short transient.

4.2.5. Case Study 5: Islanding Due to a Fault

The objective of this study was to investigate the transient behavior when a fault happens in the upstream of the system. Two sub-cases were conducted. The fault location in Case 5 was between the point 1 and the interconnection in Fig. 4.1.

In Case 5, the initial load level and power references of the DER units were the same as in Case 1. The output power references of three DER units were 20kW, 60kW+j20kVar and 40kW+j10kVar respectively. The load banks in three zones were 60kW+j20kVar, 40kW+j10kVar and 40kW+j10kVar.

a) Case 5a: Islanding due to a SLG fault

Case 5a presents the islanding process due to a SLG fault. At t = 1s, there was a single line to ground fault occurred in point 1, which is in the upstream of the interconnection switches and outside of the microgrid. The simulation stopped at t = 2.5s.

The output real power values for the DER units are shown in Fig. 4.29, and the reactive power values for the DER units are shown in Fig. 4.30. The zero sequence current and the interconnection switch status are shown in Fig. 4.31. These figures indicate that after the SLG fault happened, the protective relay 2 detected a large zero sequence current immediately and sent the trip signal to the interconnection switch. The interconnection switch opened and the microgrid transferred from the grid-connected mode into islanded mode.

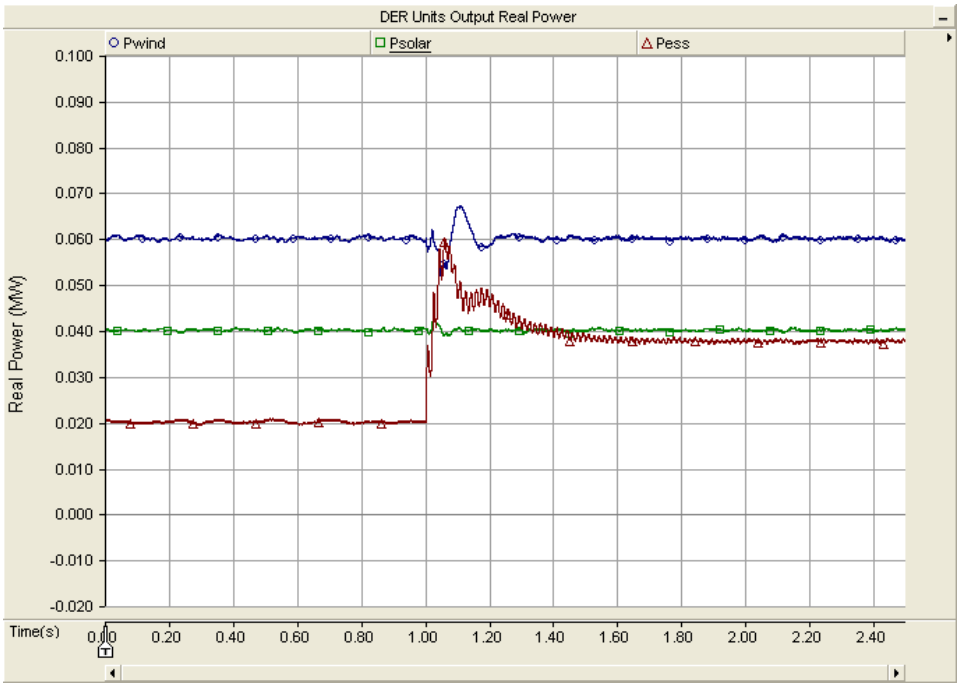

Fig. 4.29. Real power output values of DER units in Case 5a

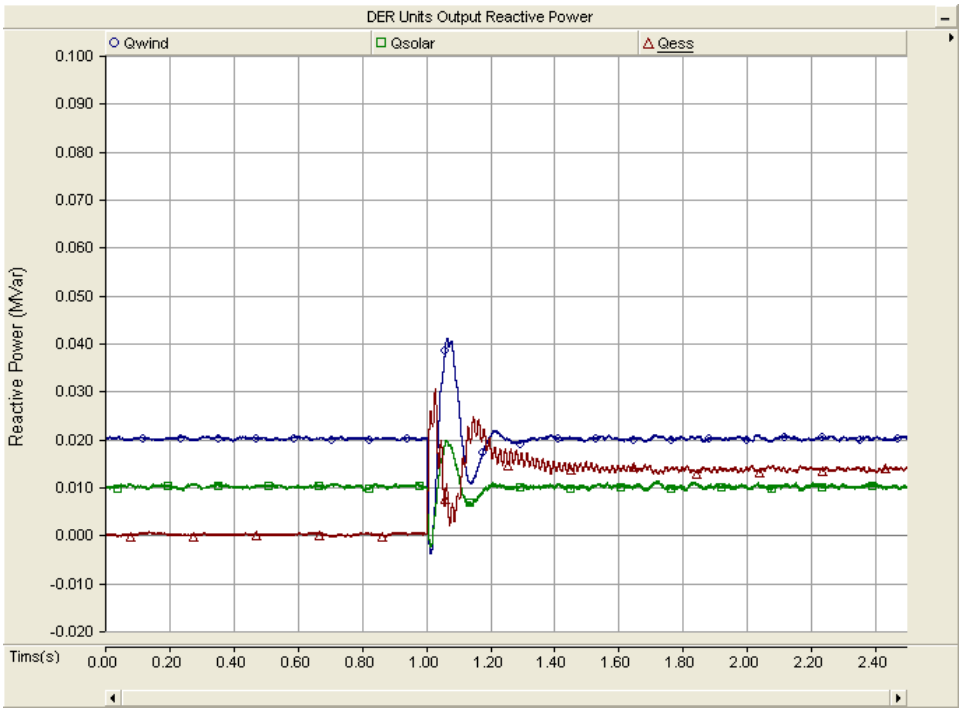

Fig. 4.30. Reactive power output values of DER units in Case 5a

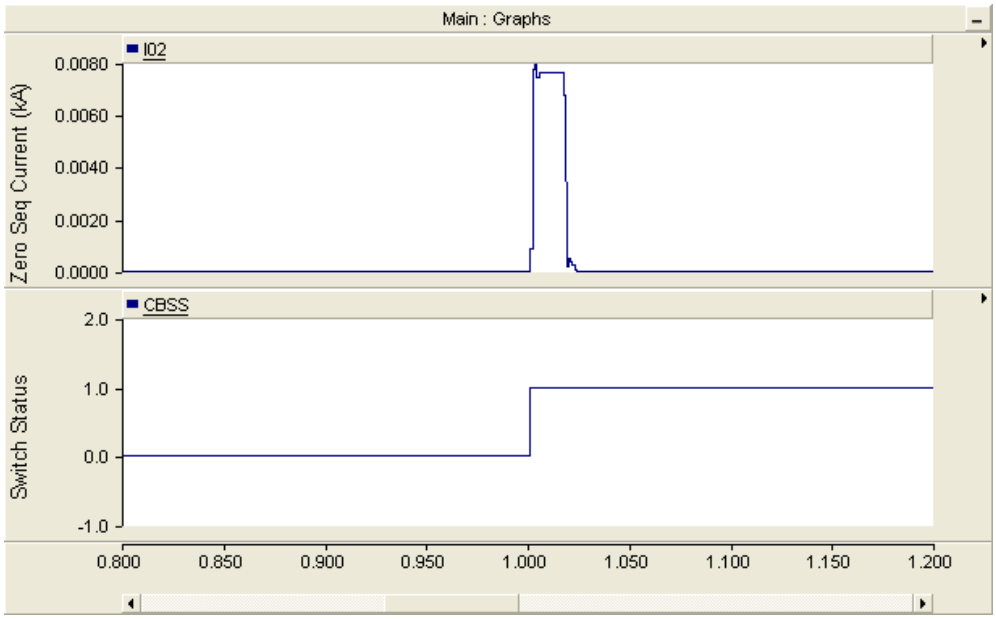

Fig. 4.31. The zero-sequence current and the interconnection switch status in Case 5a

b) Case 5b: Islanding due to a LL fault

Case 5b presents the islanding process due to a LL fault. At t = 1s, there was a line to line fault occurred outside of the microgrid. The simulation stopped at t = 2.5s. The negative sequence current and the interconnection switch status are shown in Fig. 4.32. The initial negative-sequence current was due to the harmonics existing in the system, which was smaller. When the fault occurred, the protective relay 2 detected a large negative sequence current immediately and sent the trip signal to the interconnection switch. The interconnection switch disconnected the microgrid from the utility grid, and the microgrid transferred from the grid-connected mode into islanded mode. The dynamics of other variables were very similar to those in Case 5a.

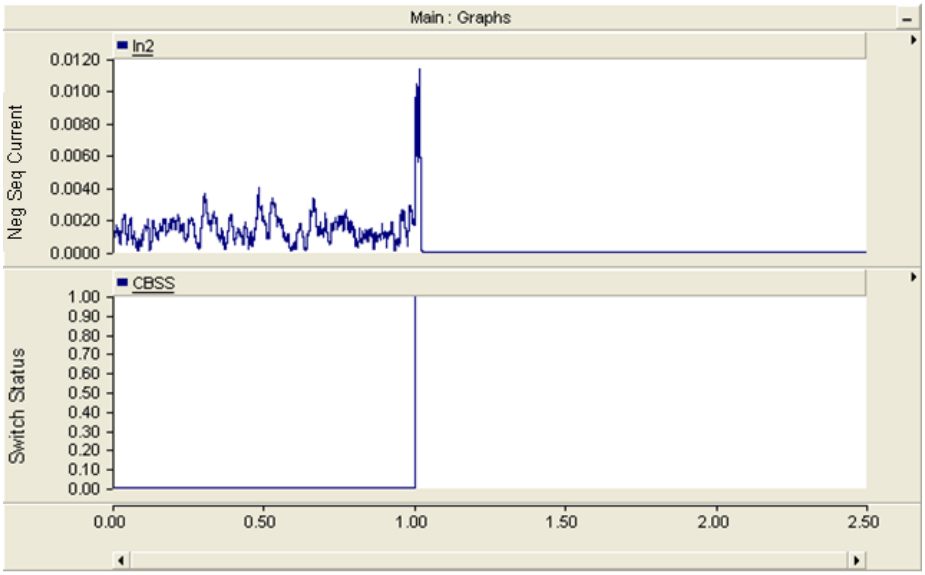

Fig. 4.32. The negative-sequence current and the interconnection switch status in Case 5b

Case 5 indicates that when a fault occurred upstream of the interconnection switches, the microgrid disconnected itself from the grid and transferred from grid-connected mode into the islanded mode.

4.2.6. Case Study 6: The Secondary Control after Islanding

Secondary control refers to the power reference values adjustment after the microgrid transfers into the islanded mode. The objective of this case study was to investigate the secondary control capability of the microgrid system. Two sub-cases were conducted.

In Case 6, the initial load level and power references of the DER units were the same as in Case 1. The output power references of the three DER units were 20kW, 60kW+j20kVar, and 40kW+j10kVar, respectively. The load banks in the three zones were 60kW+j20kVar, 40kW+j10kVar and 40kW+j10kVar.

a) Case 6a: Real power reference changes after islanding

In Case 6a, the microgrid transferred into islanded mode at t = 1s. After that, at t = 2s, the real power reference of wind energy source changed from 60kW to 70kW. At t =3s, the real power reference of solar energy source changed from 40kW to 50kW. The simulation ended at t = 5s. The output real power values for the DER units are shown in Fig. 4.33, and the output reactive power values for the DER units are shown in Fig. 4.34. Those two figures show that in the islanded mode, the real power output values of wind and solar energy source changed to the new reference values. The ESS unit output real power decreased accordingly from 40kW to 20kW.

Wind turbine output power and mechanical torque are shown in Fig. 4.35. The synchronous generator output power and mechanical speed are shown in Fig. 4.36. The PV arrays responses are shown in Fig. 4.37. These figures indicated that after the real power reference values changed, the wind and solar energy sources reached new steady state and the real power values were the same as the new reference values.

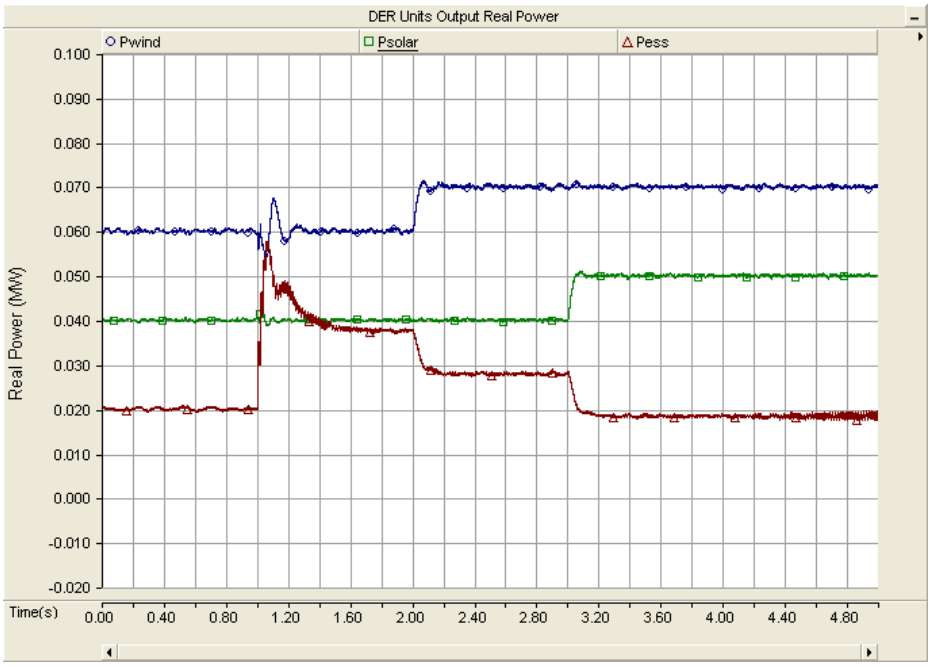

Fig. 4.33. Real power output values of DER units in Case 6a

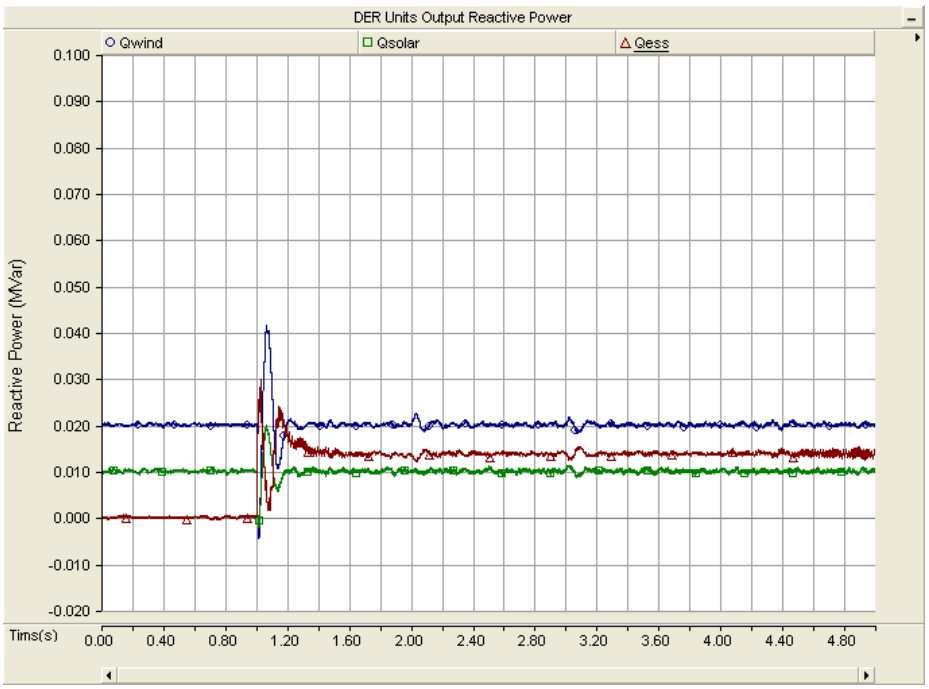

Fig. 4.34. Reactive power output values of DER units in Case 6a

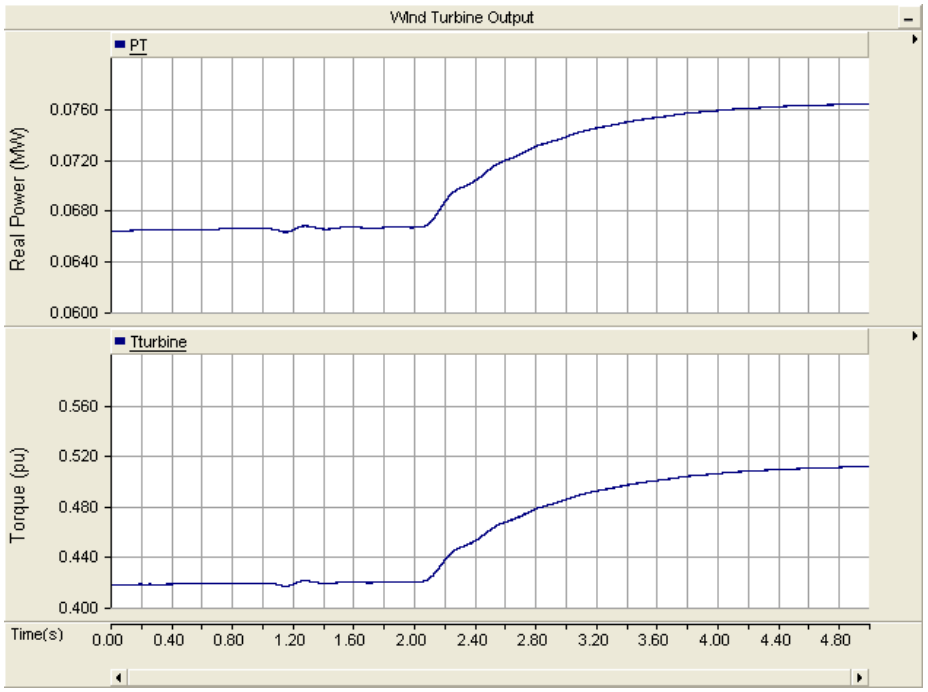

Fig. 4.35. Wind turbine output power and mechanical torque in Case 6a

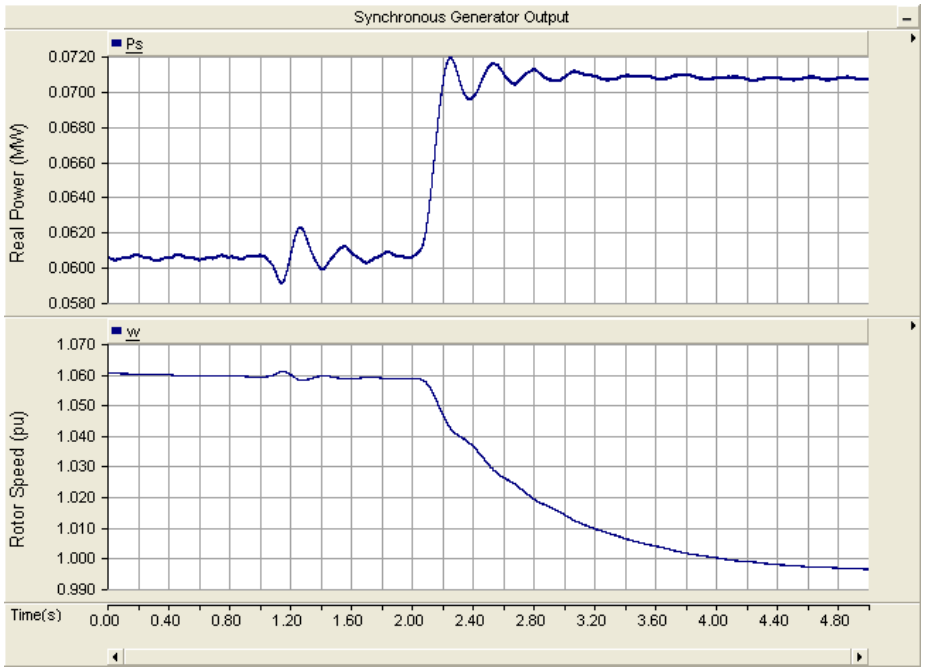

Fig. 4.36. The synchronous generator responses in Case 6a

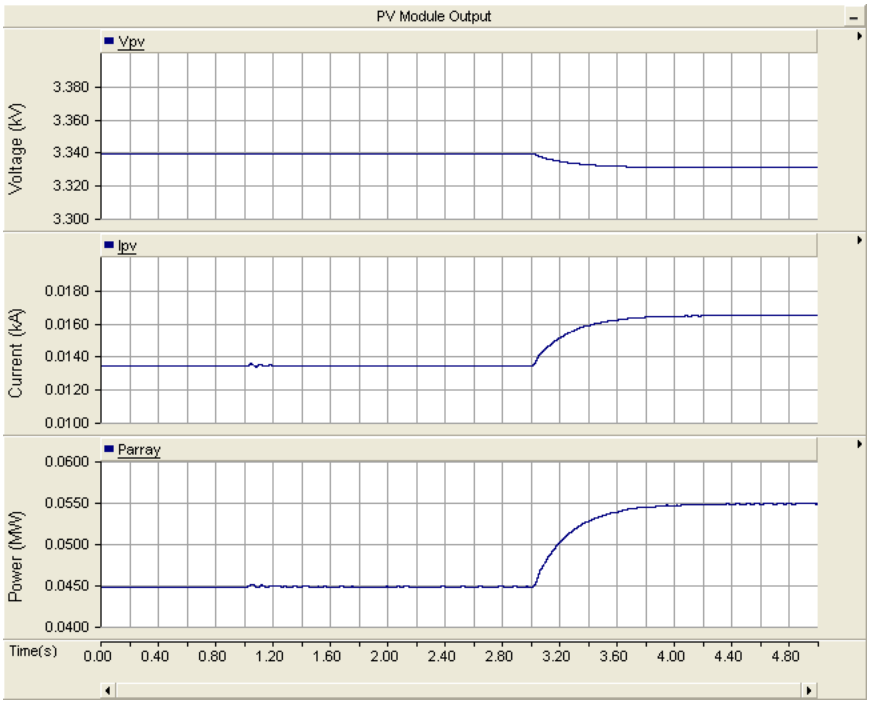

Fig. 4.37. The PV arrays responses in Case 6a

b) Case 6b: Reactive power reference changes after islanding

In Case 6b, the microgrid transferred into islanded mode at t = 1s. After that, at t = 2s, the reactive power reference of wind energy source changed from 20kVar to 10kVar. At t =3s, the reactive power reference of solar energy source changed from 10kW to 0.

The simulation stopped at t = 5s. The output real power values for the DER units are shown in Fig. 4.38, and the reactive power values for the DER units are shown in Fig. 4.39. These two figures show that in the islanded mode, the reactive power output values of wind and solar energy sources changed to the new reference values. The ESS unit output reactive power increased accordingly from 15kVar to 35kVar.

Wind turbine output power and mechanical torque are shown in Fig. 4.40. The synchronous generator output power and mechanical speed are shown in Fig. 4.41. The PV arrays responses are shown in Fig. 4.42. These figures indicate that the reactive power references adjustment did not obviously influence the wind turbine, synchronous generator and PV arrays. The wind and solar energy sources output reactive power values were the same as the new reference values.

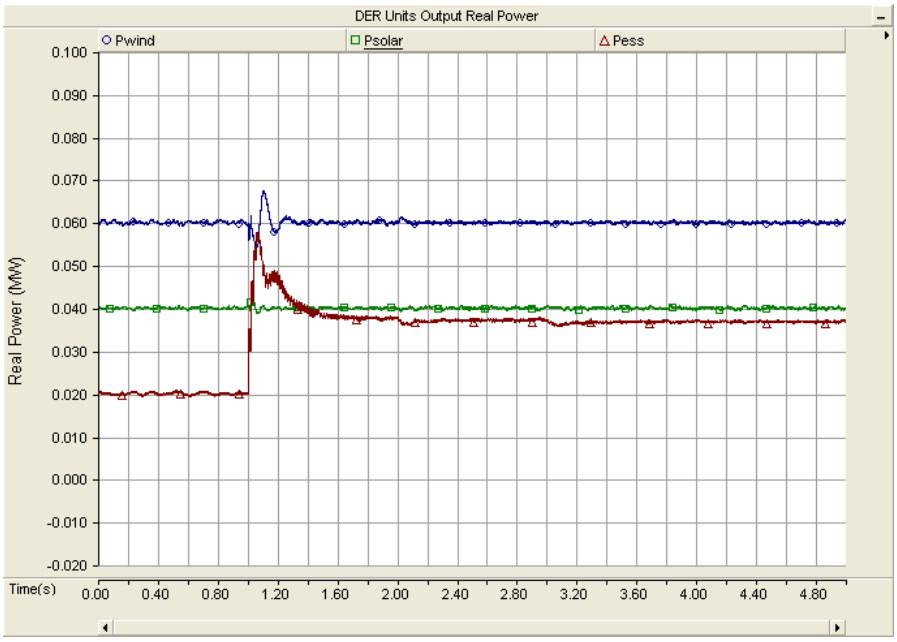

Fig. 4.38. Real Power output values of DER units in Case 6b

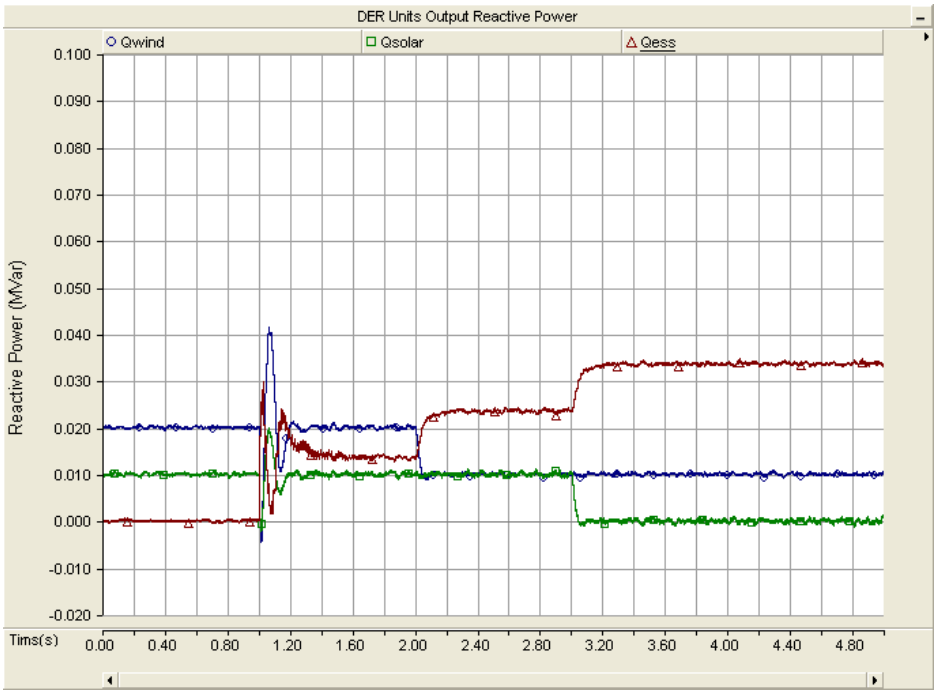

Fig. 4.39. Reactive power output values of DER units in Case 6b

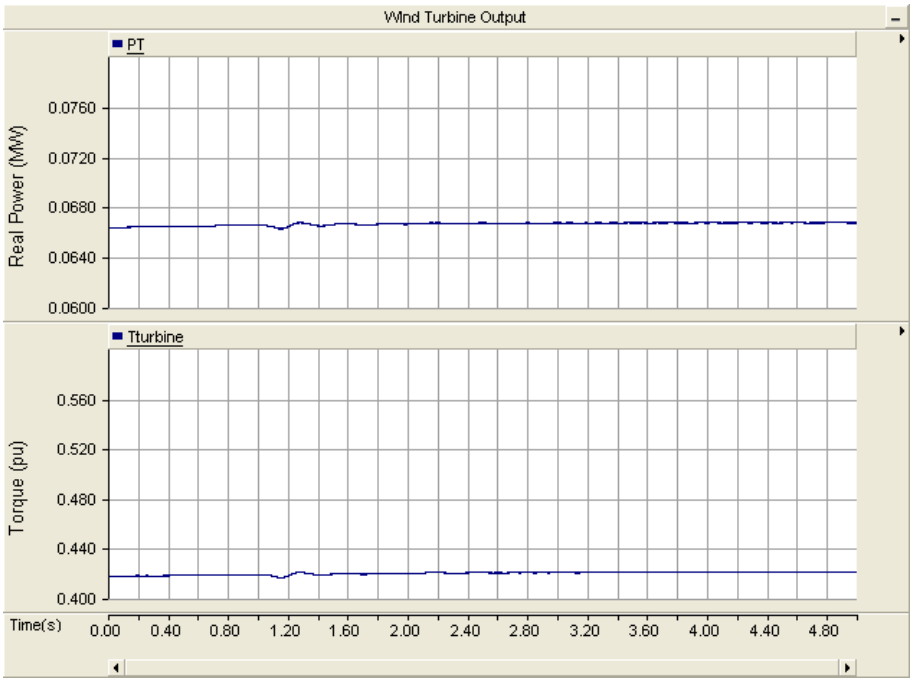

Fig. 4.40. Wind turbine output power and mechanical torque in Case 6b

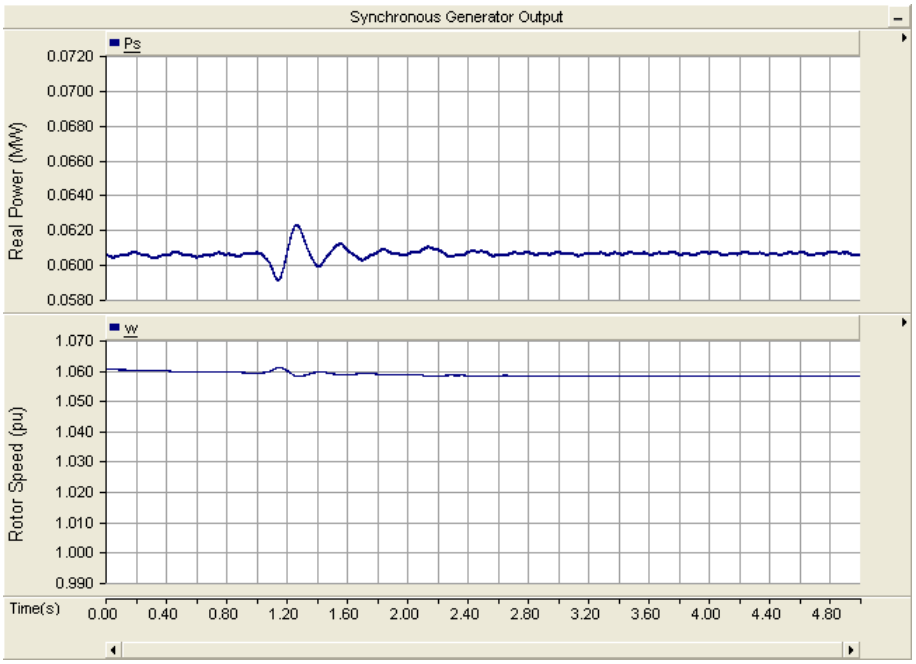

Fig. 4.41. The synchronous generator responses in Case 6b

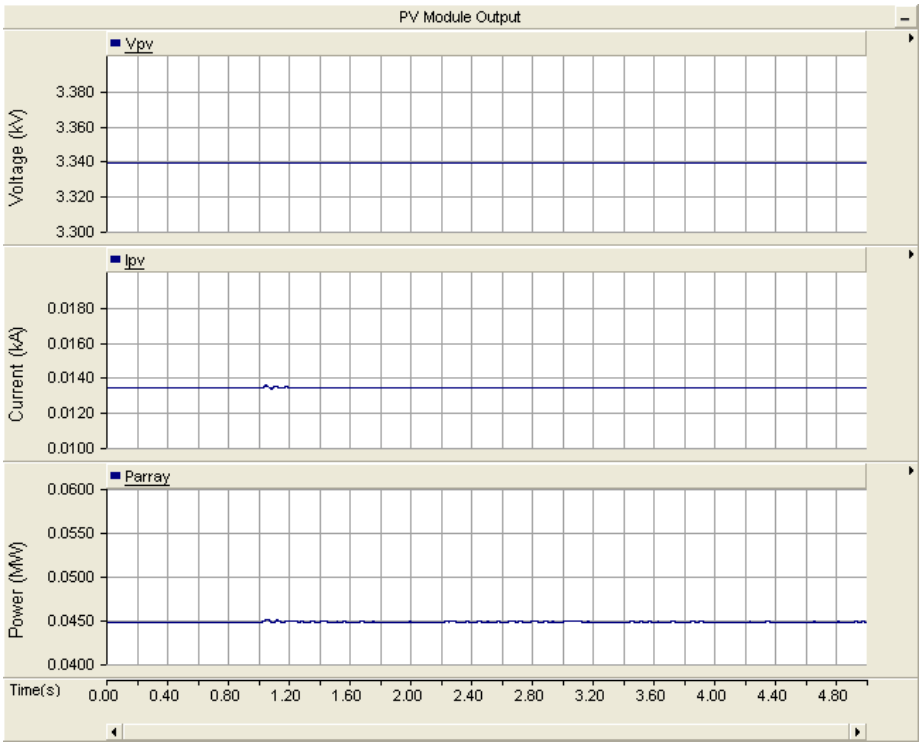

Fig. 4.42. The PV arrays responses in Case 6b

Case 6 shows that in the islanded mode, the DER units were able to perform the secondary control function. If the real or reactive power reference values changed for the wind and solar energy source, the DER units would readjust the output power to the new reference values.

5. CONCLUSIONS AND FUTURE WORK

5.1. Conclusions

A microgrid simulation model was developed in PSCAD/EMTDC software. The microgrid system model includes the fundamental power system components, the renewable energy sources and protective relays. Three DER units were modeled in this work, which were a wind energy source, a solar energy source, and an energy storage source. The PQ control methods are used in all of these three DER units. For the energy storage source, the voltage and frequency control method is also used. The microgrid system voltage was rated at 480V/277V.

Using the microgrid system model developed in this work, a group of case studies were conducted. From the results, various observations were made:

a) The PQ control method was effective to control the output power of the DER units.

b) The microgrid was able to transfer from the grid-connected into the islanded mode due to the pre-planned islanding or a fault outside a microgrid.

c) The ESS unit was able to operate in either PQ control mode or the V/F control mode. The V/F control mode enabled the ESS to maintain the system voltage level at 480V after islanding.

5.2. Future Work

The settings for the protection scheme in the microgrid were based on ideal AC sources rather than the DER units. A DER unit is different from an ideal source. For example, a DER unit has more complicated dynamic characteristics. Also a DER unit output voltage and current usually contain harmonic components. The power output of a DER unit is limited. These differences could lead the existing protection scheme to not work as expected. Therefore, the protection scheme should be enhanced in future.

Several applications and extensions can be made to the microgrid system model reported in this work. For example, the control methods of each DER units could be more deeply investigated to enable the re-synchronizing function of the interconnection switch. The re-synchronizing function should make the microgrid be able to switch from the islanded-mode into grid-connected mode without stability problems.

Another issue might be further studied is to improve the controllers of the DER units, so that the output power of the wind energy source and solar energy source can follow external conditions such as wind speed and solar radiation. The maximum power point tracking (MPPT) function could be incorporated which will maximize the efficiency of the DER units. MPPT functions for wind energy source and solar energy source could be applied into the microgrid system to achieve the advanced master control and maximize the use of the renewable energy sources.

REFERENCES

[1] B. Kroposki, R. Lasseter, T. Ise, S. Morozumi, S. Papathanassiou, and N. Hatziargyriou, "Making microgrids work," *IEEE Power Energy*, vol. 6, no. 3, pp. 40-53, May 2008.

[2] N. Miller and Z. Ye, "Report on distributed generation penetration study," National Renewable Energy Laboratory, Golden, CO, NREL/SR-560-34715, Aug. 2003.

[3] P. Piagi and R. H. Lasseter, "Microgrid: A conceptual solution," in *Proc. 2004 35th Annual IEEE Power Electronics Specialists Conf.*, pp. 4285-4290.

[4] Distibuted Energy Resources Integration Research Program, Public Interest Energy Research Program, and California Energy Commission. (Dec. 2004). "Microgrid business cases," [Online]. Available: http://www.electricdistribution.ctc.com/pdfs/Microgrid_Assessment_Phase_1.pdf. [Accessed: Oct. 2009]

[5] CERTS microgrid concept. [Online]. Available: http://certsmicrogrid.com/. [Accessed: Oct. 2009]

[6] R. H. Lasseter, "MicroGrids," in *Proc. Power Engineering Society Winter Meeting*, vol.1, pp. 305-308, Jan. 2002.

[7] Resource Dynamics Corporation. (2005, Jan.). Characterization of Microgrids in the United States. Vienna, VA. [Online]. Available: http://www.electricdistribution.ctc.com/pdfs/RDC_Microgrid_Whitepaper_1-7-05.pdf.

[8] J. Driesen and F. Katiraei, "Design for distributed energy resources," *IEEE Power Energy*, vol. 6, no. 3, pp. 30- 40, May 2008.

[9] N. R. Friedman. (2002, Sep.). "Distributed energy resources interconnection systems: Technology review and research needs," Resource Dynamics Corporation, Vienna, VA. [Online]. Available: http://www.electricdistribution.ctc.com/pdfs/32459.pdf. [Accessed: Oct. 2009]

[10] F. Ktiraei, R. Iravani, N. Hatziargyriou, and A. Dimeas. "Microgrids management - controls and operation aspects of microgrids," *IEEE Power Energy*, vol. 6, no. 3, pp. 54- 65, May 2008.

[11] J.-H. Jeon, J.-Y. Kim, S.-K. Kim, and J.-B. Ahn, "Development of HILS (Hardware In-Loop Simulation) system for MMS (Microgrid Management System) by using RTDS," in *Proc. Power Electronics and Motion Control Conf.*, pp. 2492-2497, Sep. 2008.

[12] D. M. Divan, M. C. Chandorkar, and R. Adapa, "Control of parallel connected inverters in standalone AC supply systems," *IEEE Trans. Ind. Appl.*, vol. 29, no.1, pp. 136-143, Jan. 1993.

[13] E. Joseph, R. Lasseter, B. Schenkman, J. Stevens, H. Volkommer, D. Klapp, E. Linton, H. Hurtado, J. Roy, N. J. Lewis, and Consortium for Electric Reliability Technology Solutions (CERTS). (2008). CERTS Microgrid Laboratory Test Bed. California Energy Commission and Public Interest Energy Research Program. Tech. Rep. CEC-500-2008-XXX. [Online]. Available: http://certs.lbl.gov/certs-derkey-mgtb.html. [Accessed: Oct. 2009]

[14] S. Morozumi, "Micro-grid demonstration projects in Japan," in *Proc. Power Conversion Conf.*, pp. 635-642, Apr. 2007.

[15] EU Microgrids Project. [Online]. Available: http://www.microgrids.eu. [Accessed: Oct. 2009]

[16] C. Nayar, M. Tang, and W. Suponthana, "Wind/PV/diesel micro grid system implemented in remote islands in the Republic of Maldives," in *Proc. IEEE Sustainable Energy Technologies International Conf.*, pp. 1076-1080, Nov. 2008.

[17] Renewable Energy. [Online]. Available: http://en.wikipedia.org/wiki/Renewable_energy. [Accessed: Nov. 2009]

[18] P. M. Anderson and A. Bose, "Stability simulation of wind turbine systems," *IEEE Trans. Power App. Syst.*, vol. PAS-102, no. 12, pp. 3791-3795, Dec. 1983.

[19] A. Murdoch, J. R. Winkelman, S. H. Javid, and R. S. Barton, "Control design and performance analysis of a 6 MW wind turbine-generator," *IEEE Trans. Power App. Syst.*, vol. PAS-102, no. 5, pp. 1340-1347, May 1983.

[20] P. Nema, R. K. Nema, and S. Rangnekar, "A current and future state of art development of hybrid energy system using wind and PV-solar: A review," *Renew. Sust. Energ. Rev.*, vol. 13, no. 8, pp. 2096-2103, Oct. 2009.

[21] T. Ackermann, *Wind Power in Power Systems*. Stockholm: John Wiley & Sons Ltd, 2005.

[22] M. Shahabi, M. R. Haghifam, M. Mohamadian, and S. A. Nabavi-Niaki, "Microgrid Dynamic Performance Improvement Using a Doubly Fed Induction Wind Generator," *IEEE Trans. Energy Convers.*, vol. 24, no. 1, pp. 137-145, Mar. 2009.

[23] S.-K. Kim, J.-H. Jeon, C.-H. Cho, E.-S. Kim, and J.-B. Ahn, "Modeling and simulation of a grid-connected PV generation system for electromagnetic transient analysis," *Solar Energy*, vol. 83, no. 5, pp. 664-678, May 2009.

[24] Manitoba HVDC Research Center, PSCAD/EMTDC power system simulation software users' manual, Version 4, Winnipeg, Manitoba, Canada, 2003.

[25] S.-K Kim and E.-S Kim, "PSCAD/EMTDC-based modeling and analysis of a gearless variable speed wind turbine," *IEEE Trans. Energy Convers.*, vol. 22, no. 2, pp. 421-430, Jun. 2007.

[26] IEEE Committee Report, "Computer representation of excitation systems," *IEEE Trans. Power App. Syst.*, vol. PAS-87, no. 6, pp. 1460-1464, Jun. 1968.

[27] Z. Chen and E. Spooner, "Grid power quality with variable speed wind turbines," *IEEE Trans. Energy Convers.*, vol. 16, no. 2, pp. 148-154, Jun. 2001.

[28] A. Rajapakse, "Simulation of grid connected photovoltaic systems," *Pulse - The manitoba HVDC Research Centre Journal*, pp. 6-7, Oct. 2008.

[29] J.-Y. Kim, S.-K. Kim and J.-H. Park, "Contribution of an energy storage system for stabilizing a microgrid during islanded operation," *Journal of Electrical Engineering & Technology,* vol. 4, no. 2, pp. 194-200, May 2009.

[30] R. H. Lasseter and P. Piagi. (2006, Jan.). Control and design of microgrid components. PSERC, Ithaca, NY. [Online]. Available: http://certs.lbl.go-v/pdf/microgrid-control.pdf. [Accessed: Nov. 2009]

VITA

Zhengguo Chu received his B.E. in electrical engineering in 2007 from Tsinghua University, Beijing, China. He enrolled in the master's program in electrical engineering at Texas A&M University in the fall of 2007. He joined the Power System Automation Laboratory in spring 2008. He received his M.S. in electrical engineering in May 2010. His research interests are distributed generation, microgrid and power system simulation.

Zhengguo Chu can be reached by mail at the Department of Electrical and Computer Engineering, Texas A&M University, MS 3128, College Station, TX, 77843. His email address is: chuzg03@gmail.com.